UNIVERSITÉ DE MONTRÉAL

IMPLEMENTATION OF THE SPH PROCEDURE WITHIN THE MOOSE FINITE ELEMENT FRAMEWORK

ALEXANDRE LAURIER
DÉPARTEMENT DE GÉNIE PHYSIQUE
ÉCOLE POLYTECHNIQUE DE MONTRÉAL

MÉMOIRE PRÉSENTÉ EN VUE DE L'OBTENTION
DU DIPLÔME DE MAÎTRISE ÈS SCIENCES APPLIQUÉES
(GÉNIE ÉNERGÉTIQUE)
AVRIL 2016

UNIVERSITÉ DE MONTRÉAL

ÉCOLE POLYTECHNIQUE DE MONTRÉAL

Ce mémoire intitulé:

IMPLEMENTATION OF THE SPH PROCEDURE WITHIN THE MOOSE FINITE ELEMENT FRAMEWORK

présenté par: LAURIER Alexandre
en vue de l'obtention du diplôme de: Maîtrise ès sciences appliquées
a été dûment accepté par le jury d'examen constitué de:

M. KOCLAS Jean, Ph. D., président
M. HÉBERT Alain, Doctorat, membre et directeur de recherche
M. MARLEAU Guy, Ph. D., membre et codirecteur de recherche
M. ORTENSI Javier, Ph. D., membre et codirecteur de recherche
M. CHAMBON Richard, Ph. D., membre

ACKNOWLEDGEMENTS

This project is the result of the collaboration between the Idaho National Laboratory and my research director Alain Hébert at École Polytechnique de Montréal. I would like to thank both Javier Ortensi and Alain Hébert for considering me and subsequently offering an amazing opportunity at the internship which is the subject of this thesis. I want to sincerely thank Alain for answering my repeated questions on the issues of the SPH method, leading me to realize exactly what I had accomplished during my research. I also have to thank Javier for being the amazing mentor that he was during my long stay at INL. I thank my three research directors, Alain Hébert, Guy Marleau and Javier Ortensi in their help with the redaction of this thesis, as it was a larger undertaking than I had previously thought.

During my internship, I had the opportunity of joining a research group full of amazing people and I want to thank all the members for the great work environment. I especially have to thank Javier Ortensi and Yaqi Wang for their extended help which led me to expand my knowledge and understanding of applied nuclear physics and making this such a memorable and enjoyable work experience.

I also have to thank all the other interns I have met during my internship for the friendship and great times we had during my stay in what seemed to be the middle of nowhere. You, my friends, have helped tremendously in making this research internship an amazing experience in the USA.

Finally, I thank Sophie for sticking along with me during the past 2 years of this master's degree. Although I completed this degree, you also lived it through me and I am very thankful that you were there to support me and encourage me to keep going, time and time again. The small things you do to make my life easier add up quickly, and the obtention of this degree is in part because of you. Merci.

RÉSUMÉ

Le but de ce projet de maitrise était d'implémenter la procédure SPH à l'intérieur du code de physique de réacteur du Idaho National Laboratory (INL), qui fonctionne sur le code d'éléments finis MOOSE. Précédant ce projet, le INL ne possédait pas de procédure de correction de sections efficaces, autre que l'utilisation de la méthode SPH par le code DRAGON. La création de ce projet vient du manque de flexibilité du code DRAGON dont le INL avait besoin.

L'objectif premier de ce projet fut d'implémenter la méthode SPH pour l'équation de diffusion neutronique avec la normalisation de flux traditionnelle, Selengut et "True Selengut" et d'en tester les capacités. Le deuxième visait la dérivation des équations de transport SPH ainsi que leur implémentation pour produire les premiers résultats sur des problèmes complexes. En se basant sur des articles théorisant la correction en transport, nous avons implémenté la correction SPH pour les équations de transport en calcul S_N et P_N. La correction SPH fût testée sur des assemblages de réacteur à eau pressurisée où les résultats obtenus avec la correction de transport sont simliaires mais non supérieurs à ceux obtenus avec l'équation de diffusion. Par contre, nous pensons que l'implémentation de la correction des équations de transport permettera d'obtenir des meilleurs résultats dans les problèmes où la résolution en méthode S_N ou P_N sont nécessaires.

Une conséquence additionnelle de cette recherche fût l'implémentation d'une nouvelle méthode de résolution du problème SPH non linéaire. Jusqu'au moment présent, la procédure SPH fût résolue au travers de la méthode de Picard, soit une méthode itérative de point-fixe, tandis que la nouvelle implémentation utilise la méthode "Preconditioned Jacobian-Free Newtron Krylov" (PJFNK) qui était déja présente au sein de MOOSE pour directement résoudre le probléme non linéaire. Cette nouvelle méthode de résolution présente une réduction de temps de calcul d'un facteur approchant 50 et qui genère des facteurs SPH équivalents à ceux obtenus avec la méthode itérative avec un critère de convergence très strict, soit $\epsilon < 10^{-8}$.

La méthode SPH résolue avec PJFNK permet aussi de résoudre des problèmes qui contiennent des conditions frontières de vide ou des matériaux réflecteurs, des cas où la méthode itérative traditionnelle ne peut converger. Dans les cas où la méthode PJFNK ne permet pas de converger, nous avons élaboré une méthode hybride qui combine la méthode iterative et PJFNK. Pour ce faire, la méthode itérative est utilisée pour forcer la condition initiale de la méthode PJFNK à se situer à l'intérieur du rayon de convergence des méthodes de Newton.

Cette nouvelle méthode de résolution fût testée avec grand succès sur un modèle simplifié du réacteur TREAT du INL, un problème comportant de très larges réflecteurs en graphite ainsi que des conditions frontières de vide. Pour démontrer la puissance de la méthode SPH résolue avec PJFNK sur des problémes plus communs, la correction SPH fût appliquée avec succès sur un modèle simplifié d'un coeur de réacteur à eau pressurisée suivant les normes BEAVRS, possèdant 15 assemblages ainsi que des réflecteurs en eau. Ces deux résultats ouvrent la possibilité d'utiliser la méthode SPH avec PJFNK sur des coeurs ou réacteurs entiers pour rapidement calculer des sections efficaces corrigées qui permettront de faire des calculs multi-physiques ou même évoluant dans le temps.

ABSTRACT

The goal of this thesis was to implement the SPH homogenization procedure within the MOOSE finite element framework at INL. Before this project, INL relied on DRAGON to do their SPH homogenization which was not flexible enough for their needs. As such, the SPH procedure was implemented for the neutron diffusion equation with the traditional, Selengut and true Selengut normalizations. Another aspect of this research was to derive the SPH corrected neutron transport equations and implement them in the same framework. Following in the footsteps of other articles, this feature was implemented and tested successfully with both the P_N and S_N transport calculation schemes. Although the results obtained for the power distribution in PWR assemblies show no advantages over the use of the SPH diffusion equation, we believe the inclusion of this transport correction will allow for better results in cases where either P_N or S_N are required.

An additional aspect of this research was the implementation of a novel way of solving the non-linear SPH problem. Traditionally, this was done through a Picard, fixed-point iterative process whereas the new implementation relies on MOOSE's Preconditioned Jacobian-Free Newton Krylov (PJFNK) method to allow for a direct solution to the non-linear problem. This novel implementation showed a decrease in calculation time by a factor reaching 50 and generated SPH factors that correspond to those obtained through a fixed-point iterative process with a very tight convergence criteria: $\epsilon < 10^{-8}$.

The use of the PJFNK SPH procedure also allows to reach convergence in problems containing important reflector regions and void boundary conditions, something that the traditional SPH method has never been able to achieve. At times when the PJFNK method cannot reach convergence to the SPH problem, a hybrid method is used where by the traditional SPH iteration forces the initial condition to be within the radius of convergence of the Newton method. This new method was tested on a simplified model of INL's TREAT reactor, a problem that includes very important graphite reflector regions as well as vacuum boundary conditions with great success. To demonstrate the power of PJFNK SPH on a more common case, the correction was applied to a simplified PWR reactor core from the BEAVRS benchmark that included 15 assemblies and the water reflector to obtain very good results. This opens up the possibility to apply the SPH correction to full reactor cores in order to reduce homogenization errors for use in transient or multi-physics calculations.

TABLE OF CONTENTS

LIST OF TABLES

LIST OF FIGURES

LIST OF SYMBOLS AND ABBREVIATIONS

INL	Idaho National Laboratory
MOOSE	Multiphysics Object-Oriented Simulation Environment. Framework developed at INL on which the neutronics solvers are built.
Rattlesnake	A S_N Radiation Transport Solver within the MOOSE framework
PWR	Pressurized Water Reactor
TREAT	Transient Reactor Test Facility. Air-cooled test reactor at INL
BEAVRS	Benchmark for Evaluation and Validation of Reactor Simulations
SPH	Superhomogénéisation
PJFNK	Preconditioned Jacobian Free Newton-Krylov
DRAGON	Complete lattice code developed at "École Polytechnique de Montréal".
Serpent	Montre-Carlo lattice code developed at VTT in Finland.
FEM	Finite Element Method
PETSc	Portable, Extensible Toolkit for Scientific Computation
P_N	Method (Spherical Harmonics) of solving the transport equation using a polynomial expansion of the flux.
S_N	Method (Discrete Ordinates) of solving the transport equation using an angular discretization of the angular variable $\vec{\Omega}$.
SAAF	Self-Adjoint Angular Flux formulation of the multigroup neutron transport equation.
$\phi(\vec{x})$	Flux
$\Sigma(\vec{x})$	Removal Cross Section
$\Sigma^t(\vec{x})$	Total Cross Section
$\nu\Sigma_f(\vec{x})$	Fission Cross Section
$\Sigma_s^{g\leftarrow g'}(\vec{x})$	Zeroth moment of the Scattering Cross Section
$\Sigma_{s,\ell}^{g\leftarrow g'}(\vec{x})$	$\ell^t h$ moment of the Scattering Cross Section
V_m	Volume of homogenized region m
V_{tot}	Total Volume of the problem

LIST OF APPENDICES

CHAPTER 1 INTRODUCTION

The precise modeling of nuclear reactors is a recent feat rendered possible by the advancement of computational methods based on solutions of the Boltzman transport equation (BTE) (Alain Hébert, 2016). However, nuclear reactors are still too complex to allow high resolution modeling. As such, regions within the reactor must be homogenized together to decrease the number of regions and allow for a reasonable representation without requiring too high a computational cost. However, the act of homogenizing a region usually creates errors that stem from the loss of information and fine details. There exist techniques of homogenization that aim to reduce the errors induced by said homogenization and even to correct it after the homogenization takes place. One such technique is the Superhomogénéisation method which is the subject of this thesis.

1.1 The MOOSE Framework

This research project was conducted at the Idaho National Laboratory, an energy laboratory in the U.S.A. The INL, birthplace of the first electricity producing nuclear reactor, naturally has a very strong and devoted nuclear research group. It is also the birthplace of the finite element framework MOOSE (Gaston et al., 2009), on which all of their new codes are built (Gaston et al., 2014). The appeal of MOOSE lies in its simplicity and the fact that multi-physics capabilities are easily incorporated within the code. As such, not only does INL have it's own neutronics solvers, it also has very strong multi-physics tools related to nuclear energy, such as fuel depletion and thermal hydraulics tools. However, the laboratory does not have a tool which allows for the correction of homogenized cross sections; instead they used the SPH procedure that is included within the open source "École Polytechnique de Montréal" (EPM) code, DRAGON (Marleau et al., 2014). Although DRAGON allowed corrected cross sections, this research project was put into place to further advance the research on the SPH method and allow the INL to possess it's own cross section correction tool.

The Multiphysics Object-Oriented Simulation Environment (MOOSE) is a finite-element framework with advanced multi-physics capabilities (Gaston et al., 2009). Mainly developped at INL, it is an open-source software written in object-oriented C++ that uses some of the most advanced non-linear solving methods available, found in the PETSc toolkit. (Balay et al., 2015). MOOSE is appealing as it is not only a framework, but also acts as a code development tool. Indeed, users are encouraged to contribute to the development of the code by adding new physics and capabilities within the framework (Gaston et al., 2014). These

changes, which must be approved by the main development team, help to rapidly improve this multi-physics tool. Each module, or application, within MOOSE is usually named after an animal. INL's nuclear reactor analysis code is named MAMMOTH (Gleicher et al., 2014) and encompasses other applications such as the fuels perfomance code BISON (Williamson et al., 2012) and the YAK multigroup radiation transport module which is embedded within the radiation transport solver Rattlesnake (Wang, 2013), as seen in Figure 1.1, which was taken from (Gaston et al., 2014).

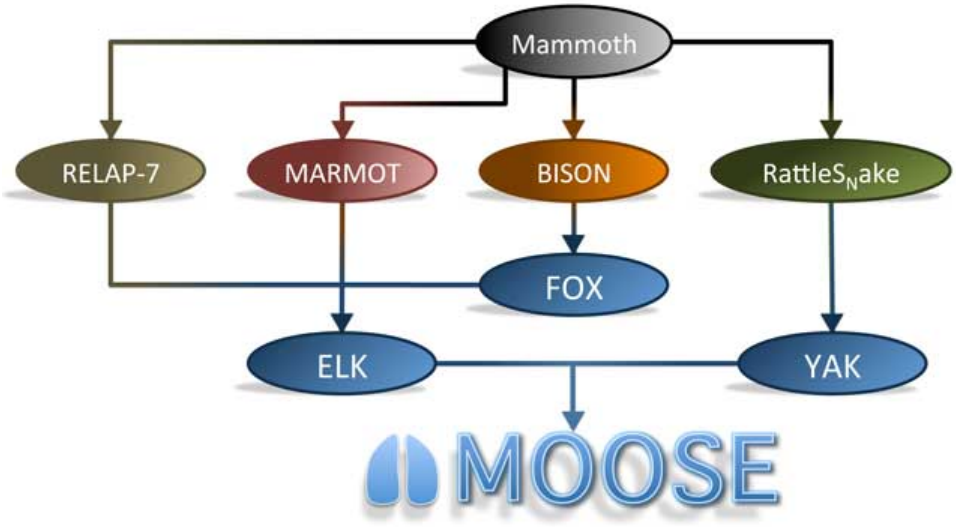

Figure 1.1 Flowchart of the dependencies between MOOSE and its applications. Image taken from (Gaston et al., 2014).

Rattlesnake was originally a radiation S_N transport application but has since evolved to include other calculations schemes such as diffusion and the P_N transport method (Wang, 2013). It now allows for many different calculation methods, such as continuous and discontinous finite-elements applied to diffusion, the SAAF formulation of the P_N and S_N transport equations and others. When a user calls for the nuclear reactor analysis code MAMMOTH, the calculation scheme is passed through Rattlesnake, which indicates to the YAK module which boundary conditions and kernels to add to the problem that will then be solved by MOOSE. The end product of MAMMOTH is straightforward; the user fills an input deck describing the mesh and the calculation scheme with a few options, calls upon MAMMOTH and automatically the problem is set up and solved by MOOSE.

1.2 Objective of the Thesis

The type of reactor analysis considered at INL requires solving the deterministic equations that govern the behaviour of neutrons. As previously mentioned, reducing the size of the problems is required for the numerical methods to be used in a realistic fashion to simulate a nuclear reactor. To do this, the infinite spectrum of neutron energy is condensed to a number of energy groups and some of the many regions within a reactor are homogenized together. Reducing the errors that stem from spatial homogenization is suggested in order to model the reactor in the most accurate way possible; the Superhomogénéisation (SPH) method is one of the tools that allow this correction.

Since the Idaho National Laboratory has such a diverse area of study when it comes to reactors, the implemented SPH method needed to be flexible, and yet robust, to account for the many types of reactors that might be designed or studied. As such, the SPH procedure was written to be a part of the MAMMOTH application within the MOOSE framework.

The first goal of the implementation of the SPH procedure within MOOSE entailed the neutron diffusion equation. There exist many pieces of literature about this specific subject and no new development was made as to the process of implementing this method. The second aspect of this research project was the derivation and application of the SPH method to the neutron transport equations for both the P_N and S_N schemes. A full derivation and testing of this method was never previously accomplished, but no reasoning existed that claimed that this implementation would not work.

Although the main goal was to apply the SPH method to the diffusion and transport equations, another primary concern at INL was its use with reflector regions. The SPH procedure is known not to converge when dealing with problems that contain large regions of reflectors or boundary conditions that are not reflective. As such, an important part of this thesis was to devise a method that would allow the correction of problems which include important reflector regions and vacuum boundary conditions.

1.3 Contents of the Thesis

In this thesis, spatial homogenization methods are reviewed and the reader is introduced to the SPH homogenization method in the literature review of Chapter 2. The basis of the SPH method is described in Chapter 3, followed by the derivation of the SPH corrected neutron diffusion and transport equations, starting at Section 3.3. The novel approach to solving the SPH problem using a Preconditioned Jacobian-Free Newton Krylov (PJFNK) method is described in chapter 3.5. Some observations about the SPH method, such as its

issues with reflectors are found in Section 3.7. Chapter 4 presents all the results generated for this thesis. This includes results pertaining to diffusion and transport SPH, as well as the comparisons with the novel PJFNK SPH method and tests run on bigger, more difficult problems. Not only has the SPH procedure shown to be well implemented, it also allows for the solution of problems which were until now unsolvable. This includes problems with large reflector regions and vacuum boundary conditions. Finally, Chapter 5 concludes the thesis, summarizing the results obtained, suggesting new research avenues for the testing of this method and presenting new ways in which the SPH method may be used. An appendix is also found that documents the derivation of the even and odd parities of the neutron transport equations.

CHAPTER 2 LITTERATURE REVIEW

2.1 Equivalence Theory

To accurately predict the behaviour of nuclear reactors, the flux distribution acquired from a fine heterogeneous calculation is required. Even though computing power is rapidly increasing, taking into account the many heterogeneous nuclear properties is still too expensive for full-core calculations. To realistically reproduce the heterogeneous results, equivalent homogenized nuclear properties, such as cross sections, are considered to act as new parameters. These equivalent parameters are used in homogenized equations to reproduce the important results such as neutron leakage, reaction rates and eigenvalues from the original heterogeneous calculation. A homogenized parameter, such as the flux or a reaction rate, within a region m is noted as:

$$\alpha_m = \frac{\int_{V_m} \alpha(\vec{r}) dV}{\int_{V_m} dV} \tag{2.1}$$

Since the behaviour of nuclear properties is greatly dependent on many factors, the homogenization process inherently leads to a loss of information when compared to the heterogeneous problem. As such, the values obtained from a homogenized calculation can only reproduce the global or averaged values from the heterogeneous scenario. Since the homogenous properties aim to reproduce the heterogeneous results of a full-core model, it is implied that the full solution is known, thus rendering the homogenization process obsolete. To circumvent this problem, heterogenous calculations are done on smaller domains of the core that produce reference values that are then used to calculate the homogenized properties. However, since each smaller domain is modelled independently of its neighbours, errors arise when the full-core problem is constructed with these new properties. As such, the introduction of new parameters to insure that the homogenized properties accurately reproduce the heterogeneous results of the full model is needed. For example, a conventional homogenization procedure consists of flux-volume weighing the cross sections, as represented by equation (2.2) where V represents the volume and ϕ the neutron flux. To generate these new cross sections, a lattice code solves the transport equation, condenses the energy groups and calculates the flux-weighed cross sections.

$$\bar{\Sigma} = \frac{\int dE \int dV \Sigma(\vec{r}, E)\phi(\vec{r}, E)}{\int dE \int dV \phi(\vec{r}, E)} \tag{2.2}$$

There are currently two widely used homogenization techniques that aim to properly reproduce the heterogeneous reactor. Both these techniques are based on equivalence theory which states that, for each macro region in the homogenized reactor calculation, the averaged fluxes and reaction rates are to be in agreement with the heterogenous calculation. For a detailed overview of the different types of homogenization methods, we direct the reader towards a state-of-the-art publication written by Sanchez (2009) or another by Smith (1986).

2.2 Generalized Equivalence Theory

The first method, expanding on equivalence theory, is called Generalized Equivalence Theory (GET) (Smith, 1986). Smith added another degree of freedom to the equations to allow the conservation of more than just averaged reaction rates and fluxes. This new parameter, called "discontinuity factor" (DF), allows for the conservation of neutron flux or currents at the boundaries. A DF is calculated at each boundary, for each energy group and is defined as:

$$f_{gik} = \frac{\bar{\phi}^{het}_{gik}}{\bar{\phi}^{hom}_{gik}}, \tag{2.3}$$

where $\bar{\phi}^{het}_{gik}$ indicates the averaged heterogeneous reference flux, in energy group g, at the boundary k of cell i. Once the DFs have been calculated, continuous homogenized fluxes can be enforced across boundaries so that:

$$\phi_{gik} f_{gik} = \phi_{gjk} f_{gjk}, \tag{2.4}$$

where k is the common boundary between cell i and j. Using this technique and flux-weighed cross sections, the transport equation is solved for the homogeneous system.

The use of DFs can also be applied to the conservation of currents by simply changing the flux to inbound or outbound currents in equations (2.3) and (2.4). Instead of preserving the averaged boundary currents, it is possible to homogenize using an assembly averaged current. This method can be done by fixing the value of the global averaged flux by multiplying the assembly surface flux by a certain constant:

$$\bar{\phi} = 4J_{\pm}, \tag{2.5}$$

from which the homogenized cross section becomes:

$$\bar{\Sigma} = \frac{\tau}{4VJ_{\pm}} \tag{2.6}$$

The application of DFs has its advantages and disadvantages. Although DFs produce good results in highly heterogeneous assemblies, the computational memory needed to do so is high,S since a DF factor must be calculated and stored for every cell surface. This heavy memory usage makes difficult the use of DF for tridimensional pin-by-pin calculations. This homogenization process also has to explicitly take into account each discontinuity factor when solving the neutron equations over the full core whereas other methods allow for simpler modifications. A limiting aspect of this method also relies with the availability of solver codes with the capability of using discontinuous fluxes to solve the neutron transport equations. In our case, the diffusion and transport calculation schemes use continuous solutions at nodes, making the use of DF impossible since every DF factor will be 1.

2.3 The Superhomogénéisation Method

The second widely used homogenization procedure, which is the main subject of this thesis, is called the Superhomogénéisation (SPH) method. First described by Kavenoky (1978) and later generalized by Hébert (Alain Hébert, 1981; Hébert and Benoist, 1991; Hébert, 1993; Hébert and Mathonnière, 1993), it introduces a new homogenization parameter, the SPH factors, to correct homogenized cross section errors. These SPH factors are applied to each averaged cross section to exactly reproduce the heterogeneous calculation's reaction rate. For each macro region and energy group, there is a unique SPH factor to be calculated and used that does not need to be further stored. This procedure is a fixed-point iterative method, which takes place between the main transport solver and the cross section modification step and thus does not require to modify the already available full-core solvers.

The neutron diffusion equation is used, henceforth, to explain the SPH method. A common practice in homogenizing a problem consists in the flux-volume weighing of cross sections for each macro region m and energy group g:

$$\bar{\Sigma}_{m,g} = \frac{\tau^{ref}_{m,g}}{V_m \phi^{ref}_{m,g}} \tag{2.7}$$

This basic case preserves the reaction rate, and to preserve more properties, such as neutron leakage, another degree of freedom is needed. The SPH factor μ is introduced, which is unique for each macro region and energy group. The averaged cross section and diffusion coefficient are corrected by applying the SPH factor as shown by equations (2.8) and (2.9):

$$\tilde{\Sigma}_{m,g} = \mu_{m,g}\bar{\Sigma}_{m,g} \tag{2.8}$$

$$\tilde{D}_{m,g} = \mu_{m,g}\bar{D}_{m,g} \tag{2.9}$$

where the SPH factors are defined as:

$$\mu_{m,g} = \frac{\phi^{ref}_{m,g}}{\tilde{\phi}_{m,g}} \tag{2.10}$$

In diffusion theory, every cross section and diffusion coefficient are to be multiplied by the SPH factor to conserve neutron balance, whereas the fluxes are to be divided by μ:

$$\tilde{\phi}_{m,g} = \frac{1}{\mu_{m,g}}\bar{\phi}_{m,g} \tag{2.11}$$

The multi-group neutron diffusion equation to be solved is then:

$$-\nabla \cdot \tilde{D}_{m,g}\nabla\tilde{\phi}_g + \tilde{\Sigma}_{m,g}\tilde{\phi}_g = \frac{\chi_g}{k_{eff}}\sum_{g'=1}^{G}\nu\tilde{\Sigma}_{f\,m,g'}\tilde{\phi}_{g'} + \sum_{g'\neq g}^{G}\tilde{\Sigma}^{g\leftarrow g'}_{s,m}\tilde{\phi}_{g'} \tag{2.12}$$

At the boundaries of the problem, a reflective boundary condition is imposed:

$$\nabla\tilde{\phi}_g \cdot \boldsymbol{N}_m = 0 \tag{2.13}$$

where $\boldsymbol{N}_m$ is the normal at the boundary of macro region m.

The SPH technique can be reduced to these few steps:

1. Calculation of the SPH factors following equation (2.10). If at the first iteration, the factors are all set to one.
2. Correction of the cross sections.
3. Solving the diffusion equation for the fluxes.
4. Normalization of the fluxes.
5. Calculation of the new SPH factors.
6. Verification of the convergence criteria between two sets of SPH factors.

If convergence of the SPH factors is not met at step 6, the procedure starts again at step 1. It is important to note that the SPH factors are to be calculated with the normalized fluxes at all times.

The use of this method is efficient for only some types of geometries. For example, the regions within the assembly to homogenize cannot be too similar, or the SPH factors become 1 and this method has no effect. In contrast, if the assembly is highly heterogeneous with important flux discrepancies, this method cannot accurately take into account these large variations, causing significant errors unless the number of homogenized regions is high enough. Otherwise, for simple assemblies, this SPH method works well to reproduce reaction rates and eigenvalues. The neutron transport equations can also be used in order to solve solve for the neutron flux in the same general manner as with the diffusion equations.

The SPH method is solved using a fixed source problem and the lack of constraints on the SPH factors allows for an infinite number of solutions. As such, a normalization condition must be imposed to obtain a unique set of SPH factors. In the original SPH technique, the averaged flux over the complete geometry is preserved by the equivalence procedure (Hébert, 1993):

$$\sum_m V_m \tilde{\phi}_{m,g} = \sum_m V_m \phi^{ref}_{m,g} \tag{2.14}$$

where V_m is the volume of region m, so that the normalized fluxes become:

$$\tilde{\phi'}_g = \tilde{\phi}_g \frac{\sum_m V_m \phi^{ref}_{m,g}}{\sum_m V_m \tilde{\phi}_{m,g}} \tag{2.15}$$

Another choice of normalization was proposed by Hébert and Mathonnière (1993) and another with the same intent by Yamamoto et al. (2004a), which can be used to improve the results for some geometries. By using the reference boundary assembly flux as the weight function for the flux normalization, flux continuity at the interface between two assemblies is ensured. This method is called Selengut normalization. Instead of using equation (2.15) at step 4 of the SPH procedure, the following normalization is used:

$$\tilde{\phi'}_g = \tilde{\phi}_g \frac{\phi^{ref,boundary}_g \sum_m V_m}{\sum_m V_m \tilde{\phi}_{m,g}} \tag{2.16}$$

Using this normalization method, the normal SPH procedure is followed to find the final homogenized flux. In more heterogeneous geometries, this method produces results that are consistent with the heterogeneous reaction rates and fluxes and is superior to the previously

proposed normalization. From this point forward, we will call this procedure the Selengut method and the previous normalization will be called the classic SPH method. When comparing the two normalization methods, the Selengut method produces the most accurate results in heterogeneous geometries where classical SPH quickly reproduces the reference reaction rates for geometries that aren't too heterogeneous. A downside with the Selengut normalization is the requirement of a reference surface flux, which is not necessarily trivial, even in Monte Carlo codes such as Serpent.

Another proposed method of conserving boundary currents with the SPH method involves the use of DFs to correct the SPH factors (Yamamoto et al., 2004a). It was recently shown (Chambon and Hébert, 2015) that this "Improved SPH method" was equivalent to the Selengut normalization: the choice of normalization can be applied during or after the iteration scheme for the same results. In this sense, it is possible to use a flux-volume normalization during the iterative scheme and then renormalize the results to preserve surface flux. The results (Yamamoto et al., 2004b,a) suggest that the improved SPH method reduces errors in highly heterogeneous calculations over the traditional SPH method. To compare the methods, a PWR colorset assembly was used but reduced to one dimension for clarity and simplicity. For less heterogeneous assemblies that are not uniform, the SPH method results in no error in the absorption rate, while in uniform assemblies the SPH factors become 1 and errors of up to 1.5% are found. For the improved SPH method, a reduction of the error was observed in assembly peripheral regions, and overall better results were obtained.

Another group (Chiba et al., 2012) further tested this improved SPH technique and compared the results with both the classical SPH and Selengut methods with the same type of reactor assembly. They found that between the improved SPH method and the Selengut normalization, the latter produced the best result: the maximum RMS error for Selengut was of 0.27% while it was 0.49% for improved SPH. The maximum errors and RMS were all higher for the improved SPH method. Selengut is also more reliable since it directly forces conservation of surface neutron flux. Another finding is that the improved SPH method produces overall better results than the classical SPH method, which is also true of the Selengut method. These results seem to indicate that using Selengut normalization is preferable for heterogeneous scenarios. While both methods require the heterogeneous assembly boundary flux, the improved SPH method requires the corrected cell surface fluxes while the Selengut method only requires the assembly boundary surface flux. Since our finite element solver easily produces the latter, only the Selengut normalization method is explored.

It was recently found (Guerin et al., 2011) that the SPH method is not fully compatible with the simplified P_N method. Guérin proposed a correction strategy that consistently corrects

the cross sections used in any P_N or simplified P_N method. Later, Hébert found that the SPH method is no more compatible with other solution techniques of the transport equation such as the collision probability (CP), interface current (IC) or method of characteristics (MOC) (Hébert, 2015). The approach proposed by Guérin and Hébert was to modify the equivalence procedure in such a way that even and odd parity cross sections and fluxes are corrected differently in a way that maintains neutron balance.

1. To maintain neutron balance, the diffusion equation becomes:

$$-\nabla\cdot\mu_{m,g}D_{m,g}\frac{\nabla\phi_g}{\mu_{m,g}}+\mu_{m,g}\Sigma_{m,g}\frac{\phi_g}{\mu_{m,g}}=\frac{\chi_g}{k_{eff}}\sum_{g'=1}^{G}\mu_{m,g'}\nu\Sigma_{f\,m,g'}\frac{\phi_{g'}}{\mu_{m,g'}}+\sum_{g'\neq g}^{G}\mu_{m,g'}\Sigma_{s,m}^{g\leftarrow g'}\frac{\phi_{g'}}{\mu_{m,g'}} \tag{2.17}$$

2. For the P_N method, balance is satisfied for even parity equations when:

$$\mu_{m,g}\Sigma_{0,m,g}^{t}\frac{\phi_{0,g}}{\mu_{m,g}}+\nabla\cdot\phi_{1,g}=\frac{\chi_g}{k_{eff}}\sum_{g'=1}^{G}\mu_{m,g'}\nu\Sigma_{f\,m,g'}\frac{\phi_{0,g'}}{\mu_{m,g'}}+\sum_{g'=1}^{G}\mu_{m,g'}\Sigma_{s,m}^{g\leftarrow g'}\frac{\phi_{0,g'}}{\mu_{m,g'}} \tag{2.18}$$

$$\frac{2\ell}{4\ell+1}\nabla\cdot\phi_{2\ell-1,g}+\mu_{m,g}\Sigma_{0,m,g}^{t}\frac{\phi_{2\ell,g}}{\mu_{m,g}}+\frac{2\ell+1}{4\ell+1}\nabla\cdot\phi_{2\ell+1,g}=\sum_{g'=1}^{G}\mu_{m,g'}\Sigma_{s,2\ell,m}^{g\leftarrow g'}\frac{\phi_{2\ell,g'}}{\mu_{m,g'}} \tag{2.19}$$

   and for odd-parity P_N equations when:

$$\frac{2\ell+1}{4\ell+3}\nabla\frac{\phi_{2\ell,g}}{\mu_{m,g}}+\frac{\Sigma_{1,m,g}^{t}}{\mu_{m,g}}\phi_{2\ell+1,g}+\frac{2\ell+2}{4\ell+3}\nabla\frac{\phi_{2\ell+2,g}}{\mu_{m,g}}=\sum_{g'=1}^{G}\frac{\Sigma_{s,2\ell+1,m}^{g\leftarrow g'}}{\mu_{m,g}}\phi_{2\ell+1,g'} \tag{2.20}$$

   where $\Sigma_{0,m,g}^{t}$ and $\Sigma_{1,m,g}^{t}$ represent the zeroth and first moment of the total cross section respectively in macro region m and energy group g.

3. If the flux is calculated from transport theory but not with a P_N method, such as with S_N, SPH correction is applied as proposed by Hébert (2015). The corrected within-group scattering cross sections are now written:

$$\tilde{\Sigma}_{s,2\ell,m}^{g\leftarrow g}=\mu_{m,g}\Sigma_{s,2\ell,m}^{g\leftarrow g}+(1-\mu_{m,g})\Sigma_{0,m,g}^{t} \tag{2.21}$$

$$\tilde{\Sigma}^{g\leftarrow g}_{s,2\ell+1,m} = \frac{\Sigma^{g\leftarrow g}_{s,2\ell+1,m}}{\mu_{m,g}} + \Big(1 - \frac{1}{\mu_{m,g}}\Big)\Sigma^{t}_{1,m,g} \tag{2.22}$$

However, no results were published using these SPH corrected equations. Another similar approach was attempted with the integro-differential neutron transport equation with some promising results for one-dimensional problems (Chiba et al., 2012).

2.4 Recent works on SPH method

2.4.1 The Super Equivalence Method

Another method based on SPH was proposed and named Super Equivalence (SPE) method (Li et al., 2014). The goal here is to force reaction rate, boundary flux and eigenvalue conservation by means of normalization. The plan is to merge the normal SPH and the improved SPH procedure with another novel normalization. To do so, the cells are homogenized and the final SPH corrective factor is calculated, named SPE factors and denoted $\omega_{m,g}$. Following this, the assembly discontinuity factor is calculated using the reference assembly heterogeneous surface flux from a Monte Carlo calculation as:

$$f_{A,g} = \frac{\phi^{ref}_{A}}{\tilde{\phi}_{A,g}} \tag{2.23}$$

The SPE factors are then corrected:

$$\omega^{P}_{m,g} = \frac{\omega_{m,k}}{f_{m,g}} \tag{2.24}$$

At this point, reaction rates are conserved from the SPH calculation, and the neutron flux is conserved by the assembly discontinuity factor. Next, conservation of the problem eigenvalue is enforced by once again modifying the SPE factor with another Monte Carlo calculated value:

$$\omega^{R}_{m,g} = \omega^{P}_{m,g}\frac{k^{hom}_{\infty}}{k^{MC}_{\infty}} \tag{2.25}$$

With this new SPE corrective factor, new cross sections, diffusion coefficients, etc. are calculated and used to solve for the final homogenized flux. The results obtained for a simplified MOX PWR core configuration show that for the standard SPH method, there is again a considerable error at the assembly peripheral regions. Results from the SPE method

are very similar to those obtained using the SPH technique, except near the assembly limits where the use of SPE factors drastically reduces the error previously observed. For a 2 and 4 group calculation, SPE produced an RMS error of 1.00% and 0.95% respectively while the classical SPH produced RMS errors of 3.64% and 0.55%. In the 4 group calculation, although the error at the boundaries of the problem is reduced with the SPE method, the RMS error is smaller with the SPH method. This might indicate a cancellation of errors in the SPE method that is not found with the SPH procedure.

2.4.2 The Iterative Semi-homogenization Method

Another method similar to SPH, called iterative semi-homogenization (ISH), aims to reproduce reaction rates and surface currents (Berman, 2013). To do so, it introduces weakly space-dependent diffusion coefficients within the cells, similar to a finer calculation meshing. As such, a cell with one cross section and diffusion coefficient is modified to contain multiple diffusion coefficients. In a one-dimensional problem, Berman uses two diffusion coefficients per cell, one for each of the boundaries surrounding the cell. The usual flux-volume weighed cross sections are used which come from a reference calculation, as well as the reference net surface current along each surface k noted $J_{g,k}$.

First, the homogenized neutron diffusion equation is solved for the flux, giving the solution noted as $\hat{\phi}^n$ for the n^{th} iteration which is then used to calculate the new cross sections and diffusion coefficients. The net surface current along the surfaces $\hat{J}^n_{g,k}$ are also calculated. It is here that the new diffusion coefficients and cross sections are introduced. The cross sections to be used for the n^{th} iterative step are defined as:

$$\hat{\Sigma}^n_g = \frac{\tau_g}{V\hat{\phi}^{n-1}_g} \tag{2.26}$$

$$\hat{D}^n_{g,1} = \hat{D}^{n-1}_{g,1}\Big(1 - \alpha\Big(1 - \frac{\hat{J}^{n-1}_{g,1}}{J_{g,1}}\Big)\Big) \tag{2.27}$$

$$\hat{D}^n_{g,2} = \hat{D}^{n-1}_{g,2}\Big(1 - \alpha\Big(1 - \frac{\hat{J}^{n-1}_{g,2}}{J_{g,2}}\Big)\Big) \tag{2.28}$$

where α is an arbitrary acceleration factor. The calculation is continued until convergence is achieved on the fluxes, cross sections and diffusion coefficients. Depending on the value of α, Berman found that the solution either diverged, or converged slowly. For example, for one dimensional (1D) tests, it was found that the SPH method converged between 5 and 10 times

faster than the ISH method. This means higher computational costs associated with this technique than traditional SPH, especially for pin-by-pin cell calculations in tridimensional geometries. Tests were performed on sets of simplified LWR cells, in 1D slabs and one energy group. As expected from the normalization, surface currents between cells were conserved, and also reproduces well the reaction rate. In all cases, the SPH method produced an exact eigenvalue while ISH led to a maximum error of 5.8%. Some tests also outline the problem the SPH method has with conserving the flux. These results also show that for highly asymmetric problems, ISH still does not perform optimally.

Some of these findings are promising for our research: the Selengut normalization method is preferred to the improved SPH method. Since the Selengut normalization requires the reference assembly boundary flux, we can also use the SPE method without large modifications to our solvers to extract the eigenvalue. Both these techniques also seemingly produce the most precise results.

2.5 Pin Power Reconstruction

An inherent downside to homogenization is the loss of information related to the original problem. With the SPH method, the fine flux distributions in the reactor are lost. A pin-by-pin power reconstruction method was proposed in Fliscounakis et al. (2011) to allow for power reconstruction for any arbitrarily homogenized geometries. The general idea is that within a pin p, the homogenized reaction rate $\bar{\tau}_p$ comes from the product between a reconstructed flux and a homogenized cross section. The reconstructed flux is a product of the homogenized diffusion flux times a shape function, which is the ratio between the transport flux $\phi_p^{t,\infty}$ and the diffusion flux $\phi_p^{d,\infty}$ calculated for a infinite medium. The reconstructed reaction rate in pin p is then:

$$\bar{\tau}_p = \bar{\Sigma}_p \bar{\phi}_p^d \frac{\phi_p^{t,\infty}}{\phi_p^{d,\infty}} \tag{2.29}$$

This method was further improved since it was found that simply using the transport and diffusion fluxes is not sufficient to produce proper power distributions (Chambon and Hébert, 2015). Chambon suggests projecting the flux distribution obtained from the reference calculation onto the polynomial flux shape obtained from the finite element solver to more accurately reproduce the pin power distribution. Here, there is no need for such pin-power reconstruction since MOOSE allows for full-core calculations with pincells, which directly produces the pin power distribution.

CHAPTER 3 THEORY

3.1 Defining the SPH factors

The Superhomogénéisation (SPH) procedure is a cross section correction method that aims to preserve total average reaction rate, leakage and eigenvalue within macro regions obtained through a homogeneous calculation with respect to a reference, heterogeneous problem (Hébert, 1993). The correction is applied to reduce the error that stems from spatial homogenization, which modifies the physics of the problem. The SPH corrected cross sections are defined as the product of the reference cross section in macro region $m \in M$, in energy group $g \in G$, with its respective SPH factor $\mu_{m,g}$. There exists a unique SPH factor for each macro region m and energy group g such that the reaction rate in these regions is preserved:

$$\Sigma_{m,g} = \mu_{m,g}\Sigma^{ref}_{m,g} \tag{3.1}$$

In equation (3.1), the superscript "ref" represents the value obtained using the condensation and homogenization process.

By definition of the SPH correction, the average reaction rate $\tau_{m,g}$ is to be preserved:

$$\tau^{ref}_{m,g} = \tau_{m,g} = \Sigma_{m,g}\phi_{m,g} = \Sigma^{ref}_{m,g}\phi^{ref}_{m,g} \tag{3.2}$$

$$\tau_{m,g} = \mu_{m,g}\Sigma^{ref}_{m,g}\phi_{m,g} = \Sigma^{ref}_{m,g}\phi^{ref}_{m,g} \tag{3.3}$$

from which the SPH factors are defined:

$$\mu_{m,g} = \frac{\phi^{ref}_{m,g}}{\phi_{m,g}}. \tag{3.4}$$

Equation (3.3) shows that the flux $\phi_{m,g}$ depends on the value of the SPH factor. As such, this non-linear system is obtained:

$$\mu_{m,g} = \frac{\phi^{ref}_{m,g}}{\phi_{m,g}(\mu_{m,g})}. \tag{3.5}$$

The determination of the SPH factors and their application will be discussed in detail in

Section 3.5. At this time, it is only important to know that these SPH factors are to be applied to the neutron transport equations, which possess $M * G$ equations of which the fluxes are the solutions. Applying the SPH method to these equations creates a system of $M * G$ equations with $M * G$ unknowns (fluxes, and thus the SPH factors). This system allows for either no solution, a unique solution or many solutions. In this case, it is easily found that an infinite number of sets of SPH factors or scaled solutions of the fluxes satisfy these equations. To constrain these values to a single set of solutions for a given problem, a new constraint parameter must be added.

3.2 SPH Normalization Schemes

The set of SPH factors presented at equation (3.3), within a certain energy group, can be divided by any factor λ_g and still preserve reaction rates. Indeed, if a cross section is divided by the said factor λ_g, the fluxes will be consequently multiplied by the same factor, as seen in equation 3.4, cancelling out the change:

$$\tau'_{m,g} = \Sigma'_{m,g}\phi'_{m,g} = \Sigma'_{m,g}\frac{\int_{V_m} dV\phi'_g}{\int_{V_m} dV} = \Sigma'_{m,g}\frac{\int_{V_m} dV\phi_g\lambda_g}{\int_{V_m} dV} = \frac{\Sigma_{m,g}}{\lambda_g}\lambda_g\phi_{m,g} = \tau_{m,g} \tag{3.6}$$

This is the same reason for the infite number of solutions to the SPH problem; any solution flux ϕ_g can be scaled by a multiplicative factor and still preserve reaction rate. To obtain a unique solution, one such multiplicative factor must be defined for each energy group. However, although scaling the fluxes within a macro region may preserve local reaction rate, it no longer preserves the total averaged reaction rate. As such, the λ is only defined for each energy group. This property can be used to define a new set of constraints that will allow only a unique set of SPH factors as a solution to the problem. These extra constraints will be added by normalizing the flux before calculating the SPH factors.

3.2.1 Flux-Volume Normalization

The traditional approach to constrain the set of factors λ is to define them in a way that preserves the domain averaged flux for each energy group g between the homogenized and reference lattice calculations (Hébert, 1993):

$$\sum_{m\epsilon M}\phi^{ref}_{m,g}V_m = \sum_{m\epsilon M}\phi'_{m,g}V_m = \sum_{m\epsilon M}\lambda_g\phi_{m,g}V_m \tag{3.7}$$

$$\bar{\phi}^{ref}_g V_{tot} = \lambda_g\sum_{m\epsilon M}\phi_{m,g}V_m = \lambda_g\bar{\phi}_g V_{tot} \tag{3.8}$$

For this type of normalization, the sets of λ_g are thus defined as:

$$\lambda_g = \frac{\bar{\phi}_g^{ref}}{\bar{\phi}_g} \tag{3.9}$$

Applying this normalization to the macro fluxes, the first set of SPH factors that define a unique solution to the problem is defined as:

$$\mu_{m,g} = \frac{\phi_{m,g}^{ref}}{\phi_{m,g}} \frac{\bar{\phi}_g}{\bar{\phi}_g^{ref}} \tag{3.10}$$

3.2.2 The Selengut Normalization

Another approach for defining a unique set of SPH factors is to add a set of constraints to guaranty flux continuity between two different assemblies (Hébert and Mathonnière, 1993; Yamamoto et al., 2004a). Following the logic behind the Flux-Volume normalization, the domain averaged flux is normalized to the reference boundary flux in each energy group. The normalization factors are then defined as:

$$\lambda_g = \frac{\phi_g^{ref,boundary}}{\bar{\phi}_g} \tag{3.11}$$

where "boundary" represents a value at the boundary of the problem. Applying this normalization to the fluxes, another unique set of SPH factors are defined:

$$\mu_{m,g} = \frac{\phi_{m,g}^{ref}}{\phi_{m,g}} \frac{\bar{\phi}_g}{\phi_g^{ref,boundary}} \tag{3.12}$$

3.2.3 The True Selengut Normalization

The Selengut method (Section 3.2.2) was initially proposed for numerical methods that could not compute the fluxes at the boundary of the domain. For the solvers within MOOSE, this is not the case. As such, the fluxes are directly normalized to preserve the actual boundary values between the reference and homogeneous problem:

$$\lambda_g = \frac{\phi_g^{ref,boundary}}{\phi_g^{boundary}}. \tag{3.13}$$

Applying this normalization to the fluxes, another unique set of SPH factors is obtained:

$$\mu_{m,g} = \frac{\phi_{m,g}^{ref}}{\phi_{m,g}} \frac{\phi_g^{boundary}}{\phi_g^{ref,boundary}}. \tag{3.14}$$

3.3 The SPH Corrected Neutron Diffusion Equation

The multi-group homogenized neutron diffusion equation is written as:

$$-\nabla \cdot D_{m,g} \nabla \phi_g + \Sigma_{m,g} \phi_g = \frac{\chi_g}{k_{eff}} \sum_{g'=1}^{G} \nu \Sigma_{f\,m,g'} \phi_{g'} + \sum_{g' \neq g}^{G} \Sigma_{s,m}^{g \leftarrow g'} \phi_{g'} \tag{3.15}$$

To preserve global reaction rate, the SPH corrected equation is (Hébert, 1993) :

$$-\nabla \cdot \mu_{m,g} D_{m,g} \frac{\nabla \phi_g}{\mu_{m,g}} + \mu_{m,g} \Sigma_{m,g} \frac{\phi_g}{\mu_{m,g}} = \frac{\chi_g}{k_{eff}} \sum_{g'=1}^{G} \mu_{m,g'} \nu \Sigma_{f\,m,g'} \frac{\phi_{g'}}{\mu_{m,g'}} + \sum_{g' \neq g}^{G} \mu_{m,g'} \Sigma_{s,m}^{g \leftarrow g'} \frac{\phi_{g'}}{\mu_{m,g'}} \tag{3.16}$$

From the previous equation, the following rules are set for the SPH correction of the neutron diffusion equation:

- The diffusion coefficient $D_{m,g}$ is multiplied by $\mu_{m,g}$.
- The removal cross section $\Sigma_{m,g}$ is multiplied by $\mu_{m,g}$.
- The scattering cross section terms $\Sigma_{s,m}^{g \leftarrow g'}$ are multiplied by $\mu_{m,g'}$.
- The fission cross section $\nu \Sigma_{f_{m,g'}}$ is multiplied by $\mu_{m.g'}$.

3.4 The SPH Corrected Neutron Transport Equation

Historically, the SPH method has been used with the neutron diffusion equation with satisfactory results. However, some problems require the use of the transport equation to obtain correct results since the approximations used to derive the diffusion equation, such as Fick's law, are no longer valid. This is the case in mediums that strongly absorb neutrons, where neutron scattering is strongly anisotropic, neutron streaming regions and in regions neighbouring a neutron source or a material surface (within a few mean free paths). This is the case in fuel rods, where the gaps also cause problems with the diffusion approximation.

Derivations of the SPH corrected neutron transport equations with the SP_N approximation have been proposed (Guerin et al., 2011; Hébert, 2015) but never tested. Chiba et al. (2012)

corrected a 1D transport equation using one energy group and found the need to only preserve the reaction rates which stem from the P_0 and P_2 components of the angular flux.

The following derivation of the SPH corrected transport equation is done through the P_N approximation since the summation notation is cleaner to work with than the integrals present in the classical transport equations. As such, the SPH corrected transport equations could have been derived using the integral notation or even through the S_N method. This means that the following derivation is also correct for any transport scheme, including S_N, Simplified P_N (SP_N) and method of characteristics (MOC).

The even and odd equations of the multi-group neutron transport equation, treated with the P_N method, are used to describe the SPH correction, which are derived in Appendix A:

$$\begin{aligned} \textit{even parity} \ : \ & \vec{\Omega}\cdot\vec{\nabla}\Psi_g^{odd}(\vec{x},\vec{\Omega}) + \Sigma_g^t(\vec{x})\Psi_g^{even}(\vec{x},\vec{\Omega}) = \\ & \sum_{g'}^{G}\sum_{\ell\ even}^{\infty}\frac{2\ell+1}{4\pi}\sum_{n=-\ell}^{\ell}\Sigma_{s,\ell}^{g\leftarrow g'}(\vec{x})\phi_{g',\ell,n}(\vec{x})Y_{\ell,n}(\vec{\Omega}) \\ & + \frac{\chi_g}{4\pi}\frac{1}{k_{eff}}\sum_{g'}^{G}\nu\Sigma_{f_{g'}}(\vec{x})\phi_{g',0,0}(\vec{x}) \end{aligned} \tag{3.17}$$

$$\begin{aligned} \textit{odd parity} \ : \ & \vec{\Omega}\cdot\vec{\nabla}\Psi_g^{even}(\vec{x},\vec{\Omega}) + \Sigma_g^t(\vec{x})\Psi_g^{odd}(\vec{x},\vec{\Omega}) = \\ & \sum_{g'}^{G}\sum_{\ell\ odd}^{\infty}\frac{2\ell+1}{4\pi}\sum_{n=-\ell}^{\ell}\Sigma_{s,\ell}^{g\leftarrow g'}(\vec{x})\phi_{g',\ell,n}(\vec{x})Y_{\ell,n}(\vec{\Omega}) \end{aligned} \tag{3.18}$$

where the even and odd moments of the flux are defined as:

$$\Psi_g^{even}(\vec{x},\vec{\Omega}) = \frac{\Big(\Psi_g(\vec{x},\vec{\Omega}) + \Psi_g(\vec{x},-\vec{\Omega})\Big)}{2} \tag{3.19}$$

$$\Psi_g^{odd}(\vec{x},\vec{\Omega}) = \frac{\Big(\Psi_g(\vec{x},\vec{\Omega}) - \Psi_g(\vec{x},-\vec{\Omega})\Big)}{2} \tag{3.20}$$

and where $\phi_{g,\ell,n}$ follows the definition of the spherical harmonics:

$$\int_{4\pi} d\Omega'\Sigma_x^g(\vec{x},\vec{\Omega}',\vec{\Omega})\Psi_g(\vec{x},\vec{\Omega}') = \sum_{\ell=0}^{\infty}\frac{2\ell+1}{4\pi}\sum_{n=-\ell}^{\ell}\Sigma_{x,\ell}^g(\vec{x})\phi_{g,\ell,n}(\vec{x})Y_{\ell,n}(\vec{\Omega}) \tag{3.21}$$

The equations (3.17) and (3.18) are now homogenized to replace the space variable $\vec{x}$ by the region index m, and the use of $\vec{\Omega}$ for denoting spatial dependence of the variables is dropped:

$$\begin{aligned} even\ parity\ :\ \vec{\Omega}\cdot\vec{\nabla}\Psi_g^{odd} + \Sigma_{m,g}^t\Psi_g^{even} = \\ \sum_{g'}^{G}\sum_{\ell\ even}^{\infty}\frac{2\ell+1}{4\pi}\sum_{n=-\ell}^{\ell}\Sigma_{s,\ell,m}^{g\leftarrow g'}\phi_{g',\ell,n}Y_{\ell,n} \\ + \frac{\chi_g}{4\pi}\frac{1}{k_{eff}}\sum_{g'}^{G}\nu\Sigma_{f_{g'}}\phi_{g',0,0} \end{aligned} \tag{3.22}$$

$$\begin{aligned} odd\ parity\ :\ \vec{\Omega}\cdot\vec{\nabla}\Psi_g^{even} + \Sigma_{m,g}^t\Psi_g^{odd} = \\ \sum_{g'}^{G}\sum_{\ell\ odd}^{\infty}\frac{2\ell+1}{4\pi}\sum_{n=-\ell}^{\ell}\Sigma_{s,\ell,m}^{g\leftarrow g'}\phi_{g',\ell,n}Y_{\ell,n} \end{aligned} \tag{3.23}$$

Equations (3.22) and (3.23) are now used to determine the best way of applying the SPH factors. The goal of the SPH method is to preserve global reaction rates, which stems primarily from the zeroth (even) moments of the angular flux (Guerin et al., 2011). Using this fact, the SPH correction is first only applied to the cross sections and even fluxes that appear in the even equations[1]: the cross sections are multiplied and the even fluxes divided by their respective SPH factors.

$$\begin{aligned} even\ parity\ :\ \vec{\Omega}\cdot\vec{\nabla}\Psi_g^{odd} + \mu_{m,g}\Sigma_{m,g}^t\frac{\Psi_g^{even}}{\mu_{m,g}} = \\ \sum_{g'}^{G}\sum_{\ell\ even}^{\infty}\frac{2\ell+1}{4\pi}\sum_{n=-\ell}^{\ell}\mu_{m,g'}\Sigma_{s,\ell,m}^{g\leftarrow g'}\frac{\phi_{g',\ell,n}}{\mu_{m,g'}}Y_{\ell,n} \\ + \frac{\chi_g}{4\pi}\frac{1}{k_{eff}}\sum_{g'}^{G}\mu_{m,g'}\nu\Sigma_{f_{g'}}\frac{\phi_{g',0,0}}{\mu_{m,g'}} \end{aligned} \tag{3.24}$$

By preserving the contribution to the reaction rates from the even moments, all the even fluxes have to be divided by μ. This change also propagates to the odd equations which become:

[1]This was a decision we took as there seems to be no physical explanation as to the flux moments we consider in the reaction rate. However, we have discovered that preserving only the zeroth flux moment's contribution to the reaction rate does not allow for a valid SPH correction.

$$odd\ parity\ :\ \vec{\Omega}\cdot\vec{\nabla}\frac{\Psi_g^{even}}{\mu_{m,g}}+\Sigma_{m,g}^{t}\Psi_g^{odd}= \sum_{g'}^{G}\sum_{\ell\ odd}^{\infty}\frac{2\ell+1}{4\pi}\sum_{n=-\ell}^{\ell}\Sigma_{s,\ell,m}^{g\leftarrow g'}\phi_{g',\ell,n}Y_{\ell,n} \tag{3.25}$$

At this point, only the cross sections in the even equations were modified. Since the correction does not yet apply to the cross sections in the odd equations, the reaction rate pertaining to these equations is no longer conserved. To do so, every other term of these equations must be divided by $\mu_{m,g}$:

$$odd\ parity\ :\ \vec{\Omega}\cdot\vec{\nabla}\frac{\Psi_g^{even}}{\mu_{m,g}}+\frac{1}{\mu_{m,g}}\Sigma_{m,g}^{t}\Psi_g^{odd}= \frac{1}{\mu_{m,g}}\sum_{g'}^{G}\sum_{\ell\ odd}^{\infty}\frac{2\ell+1}{4\pi}\sum_{n=-\ell}^{\ell}\Sigma_{s,\ell,m}^{g\leftarrow g'}\phi_{g',\ell,n}Y_{\ell,n} \tag{3.26}$$

These equations correspond to the SPH corrected transport equations. Although this derivation was done through the P_N approximation, this correction scheme is valid for any other transport method. At this point, the infinite sum over all moments must be truncated to a certain order N to allow for a numerical solution to the problem using spherical harmonics.

Another attempt at the derivation of the SPH neutron transport equation has been tried without success. Whereas the previous derivation had the reaction rates conserved within all the even transport equations, such as in equation (3.24), this other derivation demanded that only the zeroth moment of the reaction rate is preserved. This was accomplished by seperating out the zeroth moment of the flux from the rest of the even moments. Using the same derivation method used previously, a different SPH corrected transport equation was obtained which was tested to show that it did not preserve reaction rate. Since the primary source of reaction rate stems from the zeroth (even) moments of the angular flux, there was no attempt to derive an SPH corrected transport equation where only the reaction rate stemming from the odd moments of the flux was preserved.

It is important to note that the total cross section in the even and odd equations are corrected differently; in the even equation (3.24) the total cross section is multiplied by μ whereas in the odd equation (3.26) the total cross section is divided by μ. This is because we can not enforce conservation on both the even and odd moments of the angular flux at the same time. This may cause issues in solvers that do not differentiate between the moments of the

total cross section, as is the case within Rattlesnake. If this is the case, a modification to the SPH corrected transport equations is needed to allow for a unique correction to the total cross section.

3.4.1 Modifying the Total Cross Section

If a modification to the SPH corrected transport equations is in fact needed, we suggest two correction schemes which are mathematically equivalent. The first consists in having the total cross section multiplied by μ, in the fashion of the traditionnal SPH method. To do so, the following terms must be added to both sides of the odd SPH corrected transport equations (3.26):

$$\mu_{m,g}\Sigma^t_{m,g}\Psi^{odd}_g - \frac{\Sigma^t_{m,g}\Psi^{odd}_g}{\mu_{m,g}} \tag{3.27}$$

to obtain:

$$\begin{aligned} odd\ parity\ :\ \vec{\Omega}\cdot\vec{\nabla}\frac{\Psi^{even}_g}{\mu_{m,g}} + \mu_{m,g}\Sigma^t_{m,g}\Psi^{odd}_g = \\ \frac{1}{\mu_{m,g}}\sum_{g'}^{G}\sum_{\ell\ odd}^{N}\frac{2\ell+1}{4\pi}\sum_{n=-\ell}^{\ell}\Sigma^{g\leftarrow g'}_{s,\ell,m}\phi_{g',\ell,n}Y_{\ell,n} \\ + \Sigma^t_{m,g}\Psi^{odd}_g\Big(\mu_{m,g} - \frac{1}{\mu_{m,g}}\Big) \end{aligned} \tag{3.28}$$

The angular flux ,Ψ^{odd}_g, on the right-hand side of the equation is expanded into its components:

$$\begin{aligned} odd\ parity\ :\ \vec{\Omega}\cdot\vec{\nabla}\frac{\Psi^{even}_g}{\mu_{m,g}} + \mu_{m,g}\Sigma^t_{m,g}\Psi^{odd}_g = \\ \sum_{g'}^{G}\sum_{\ell\ odd}^{N}\frac{2\ell+1}{4\pi}\sum_{n=-\ell}^{\ell}\frac{\Sigma^{g\leftarrow g'}_{s,\ell,m}}{\mu_{m,g}}\phi_{g',\ell,n}Y_{\ell,n} \\ + \sum_{\ell\ odd}^{N}\frac{2\ell+1}{4\pi}\sum_{n=-\ell}^{\ell}\Sigma^t_{m,g}(\mu_{m,g} - \frac{1}{\mu_{m,g}})\phi_{g',\ell,n}Y_{\ell,n} \end{aligned} \tag{3.29}$$

to finally include the last term in the within group scattering using a Kronecker delta to obtain:

$$odd\ parity\ :\ \vec{\Omega}\cdot\vec{\nabla}\frac{\Psi_g^{even}}{\mu_{m,g}}+\mu_{m,g}\Sigma_{m,g}^{t}\Psi_g^{odd}= \tag{3.30}$$
$$\sum_{g'}^{G}\sum_{\ell\ odd}^{N}\frac{2\ell+1}{4\pi}\sum_{n=-\ell}^{\ell}\Big(\frac{\Sigma_{s,\ell,m}^{g\leftarrow g'}}{\mu_{m,g}}+\delta_{g,g'}\Sigma_{m,g}^{t}(\mu_{m,g}-\frac{1}{\mu_{m,g}})\Big)\phi_{g',\ell,n}Y_{\ell,n}$$

From the combination of the even (3.24) and odd (3.30) equations, we get the following rules for the SPH correction for the neutron transport equation:

- The total cross section $\Sigma_{m,g}^{t}$ is multiplied by $\mu_{m,g}$.
- The fission cross section $\nu\Sigma_{f_{m,g'}}$ is multiplied by $\mu_{m,g'}$.
- For ℓ even, the scattering cross section terms $\Sigma_{s,\ell,m}^{g\leftarrow g'}$ are multiplied by $\mu_{m,g'}$.
- for ℓ odd, the scattering cross section terms are corrected as:
  $\Sigma_{s,\ell,m}^{g\leftarrow g'}\rightarrow\frac{\Sigma_{s,\ell,m}^{g\leftarrow g'}}{\mu_{m,g}}+\delta_{g,g'}\Sigma_{m,g}^{t}(\mu_{m,g}-\frac{1}{\mu_{m,g}})$.

3.4.2 Not Modifying the Total Cross Section

The second correction scheme suggested for the application of the SPH corrected transport equation relies on not modifying the total cross section. To do so, the same logic as in Section 3.4.1 is applied, where the following terms are added to the odd SPH corrected transport equations (3.26):

$$\Sigma_{m,g}^{t}\Psi_g^{odd}-\frac{\Sigma_{m,g}^{t}}{\mu_{m,g}}\Psi_g^{odd} \tag{3.31}$$

to obtain:

$$odd\ parity\ :\ \vec{\Omega}\cdot\vec{\nabla}\frac{\Psi_g^{even}}{\mu_{m,g}}+\Sigma_{m,g}^{t}\Psi_g^{odd}= \tag{3.32}$$
$$\frac{1}{\mu_{m,g}}\sum_{g'}^{G}\sum_{\ell\ odd}^{N}\frac{2\ell+1}{4\pi}\sum_{n=-\ell}^{\ell}\Sigma_{s,\ell,m}^{g\leftarrow g'}\phi_{g',\ell,n}Y_{\ell,n}$$
$$+\Sigma_{m,g}^{t}\Psi_g^{odd}\Big(1-\frac{1}{\mu_{m,g}}\Big)$$

Since the total cross section is no longer modified, the even equations (3.24) must also be changed:

$$
\begin{aligned}
even\ parity\ :\ \vec{\Omega}\cdot\vec{\nabla}\Psi_g^{odd} + \Sigma_{m,g}^t \frac{\Psi_g^{even}}{\mu_{m,g}} = \\
&\sum_{g'}^{G}\sum_{\ell}^{N}\sum_{even}\frac{2\ell+1}{4\pi}\sum_{n=-\ell}^{\ell}\mu_{m,g'}\Sigma_{s,\ell,m}^{g\leftarrow g'}\frac{\phi_{g',\ell,n}}{\mu_{m,g'}}Y_{\ell,n} \\
&+\frac{\chi_g}{4\pi}\frac{1}{k_{eff}}\sum_{g'}^{G}\mu_{m,g'}\nu\Sigma_{f_{g'}}\frac{\phi_{g'}}{\mu_{m,g'}} \\
&+\Sigma_{m,g}^t\frac{\Psi_g^{even}}{\mu_{m,g}}\Big(1-\mu_{m,g}\Big)
\end{aligned}
\tag{3.33}
$$

where Ψ_g^{even} and Ψ_g^{odd} in the previous equations are now expanded in their components and combined in the within group scattering:

$$
\begin{aligned}
even\ parity\ :\ \vec{\Omega}\cdot\vec{\nabla}\Psi_g^{odd} + \Sigma_{m,g}^t \frac{\Psi_g^{even}}{\mu_{m,g}} = \\
&\sum_{g'}^{G}\sum_{\ell}^{N}\sum_{even}\frac{2\ell+1}{4\pi}\sum_{n=-\ell}^{\ell}\Big(\mu_{m,g'}\Sigma_{s,\ell,m}^{g\leftarrow g'}+\delta_{g,g'}\Sigma_{m,g}^t(1-\mu_{m,g})\Big)\frac{\phi_{g',\ell,n}}{\mu_{m,g'}}Y_{\ell,n} \\
&+\frac{1}{k_{eff}}\frac{\chi_g}{4\pi}\sum_{g'}^{G}\mu_{m,g'}\nu\Sigma_{f_{m,g'}}\frac{\phi_{g'}}{\mu_{m,g'}}
\end{aligned}
\tag{3.34}
$$

$$
\begin{aligned}
odd\ parity\ :\ \vec{\Omega}\cdot\vec{\nabla}\frac{\Psi_g^{even}}{\mu_{m,g}} + \Sigma_{m,g}^t \Psi_g^{odd} = \\
&\sum_{g'}^{G}\sum_{\ell}^{N}\sum_{odd}\frac{2\ell+1}{4\pi}\sum_{n=-\ell}^{\ell}\Big(\frac{\Sigma_{s,\ell,m}^{g\leftarrow g'}}{\mu_{m,g}}+\delta_{g,g'}\Sigma_{m,g}^t(1-\frac{1}{\mu_{m,g}})\Big)\phi_{g',\ell,n}Y_{\ell,n}
\end{aligned}
\tag{3.35}
$$

This correction scheme does not modify the total cross sections, and the correction required by the equivalence relations are transfered to the within group scattering terms. These two methods of cross section corrections are mathematically equivalent, assuming a summation over infinite values of N. The cross sections are corrected following these rules:

- The total cross section $\Sigma_{m,g}^t$ is not modified.
- The fission cross section $\nu\Sigma_{f_{m,g'}}$ is multiplied by $\mu_{m,g'}$.
- for ℓ even, the scattering cross section terms are corrected as:
  $\Sigma_{s,\ell,m}^{g\leftarrow g'} \rightarrow \mu_{m,g'}\Sigma_{s,\ell,m}^{g\leftarrow g'} + \delta_{g,g'}\Sigma_{m,g}^t(1-\mu_{m,g})$.

- for ℓ odd, the scattering cross section terms are corrected as:
  $\Sigma^{g\leftarrow g'}_{s,\ell,m} \rightarrow \frac{\Sigma^{g\leftarrow g'}_{s,\ell,m}}{\mu_{m,g}} + \delta_{g,g'}\Sigma^{t}_{m,g}(1 - \frac{1}{\mu_{m,g}})$.

3.5 Obtaining the SPH factors

The process of obtaining the SPH factors will only be explained with the diffusion equation, as the method is the same with the neutron transport equation. As seen in equation (3.5), the determination of the SPH factors is done through a nonlinear system of equations.

3.5.1 Iterative Process

The traditional way to obtain the SPH factors relies on a Picard, fixed-point, iterative process (Fujita et al., 2015; Yamamoto et al., 2004a; Chiba et al., 2012; Hébert, 2015; Guerin et al., 2011; Li et al., 2014; Grundmann and Mittag, 2011; Nikitin et al., 2015; Ma et al., 2015). The neutron diffusion equation with SPH corrected cross sections is used:

$$-\nabla \cdot \mu_{m,g} D_{m,g} \nabla \phi_g + \mu_{m,g}\Sigma_{m,g}\phi_g = \frac{\chi_g}{k_{eff}} \sum_{g'=1}^{G} \mu_{m,g'}\nu\Sigma_{f\,m,g'}\phi_{g'} + \sum_{g'\neq g}^{G} \mu_{m,g'}\Sigma^{g\leftarrow g'}_{s,m}\phi_{g'} \qquad (3.36)$$

The SPH procedure is described by these steps:

0. A reference calculation is performed to obtain the reference cross sections, k_{eff}, χ_g and averaged fluxes $\phi^{ref}_{m,g}$.
1. The SPH factors are applied to the equation. For the first iteration, we set $\mu^{(0)}_{m,g} = 1$.
2. Using the previous iteration's normalized flux solution, the source term (right-hand side of the equation) is calculated. For the first iteration, we use the reference averaged fluxes as source fluxes[2].
3. The left-hand side of the equation is solved for ϕ_g.
4. Using a normalization scheme (see equations (3.10), (3.12) and (3.14)), the solution fluxes are normalized.
5. Using the normalized fluxes, the SPH factors are calculated using equation (3.5).

[2]In our case, the YAK module sets the initial flux at the nodes sharing multiple regions to be equal to the average of the fluxes in those regions.

6. The convergence of every SPH factor is verified using this equation:

$$\frac{|\mu_{m,g}^{(n+1)} - \mu_{m,g}^{(n)}|}{\mu_{m,g}^{(n+1)}} \leq \epsilon \tag{3.37}$$

ϵ is usually taken to be smaller than 10^{-4}. If this criterion is not true for every SPH factor, we repeat from step 1.

3.5.2 Preconditioned Jacobian-Free Newton Krylov SPH Method

We direct the interested reader to a review of the Jacobian-Free Newton Krylov method (Knoll and Keyes, 2004) as it is not the main subject of this thesis. The MOOSE framework uses a Preconditioned Jacobian-Free Newton Krylov (PJFNK) solver as the default option to evaluate solutions to non-linear problems. This capability was used to attempt to solve the SPH equations in a novel fashion.

The Jacobian-Free Newton Krylov (JFNK) method is a fully-coupled, multi-level alrogithm for solving large non-linear equation systems. In the case at MOOSE, it consists of two levels: an outer Newton loop for the non-linear solve and an inner Krylov loop for the linear system of equations that come from the Newton iteration (Berry et al., 2014). The finite-element notation used for the system of equations is:

$$\boldsymbol{F}(\boldsymbol{u}) = 0 \tag{3.38}$$

where $\boldsymbol{u}$ is the solution vector. At the k^{th} iteration, the residual vector $\boldsymbol{r}^k$, which is to be minimized, is defined as:

$$\boldsymbol{r}^k \equiv \boldsymbol{F}(\boldsymbol{u}^k) \tag{3.39}$$

The Newton iteration procudes a Taylor expansion around the point $\boldsymbol{u}^k$, ignoring the high order terms:

$$\boldsymbol{F}(\boldsymbol{u}^{k+1}) = \boldsymbol{F'}(\boldsymbol{u}^k)(\boldsymbol{u}^{k+1} - \boldsymbol{u}^k) \tag{3.40}$$

To update the solution vector, the following equation must be solved for the change vector $\delta\boldsymbol{u}^{k+1} = \boldsymbol{u}^{k+1} - \boldsymbol{u}^k$:

$$\begin{aligned} \boldsymbol{J}(\boldsymbol{u}^k)\delta\boldsymbol{u}^{k+1} &= -\boldsymbol{r}^k \\ &= -\boldsymbol{F}(\boldsymbol{u}^k) \end{aligned} \tag{3.41}$$

where $\boldsymbol{J}(\boldsymbol{u}^k)$ is the Jacobian matrix evaluated at $\boldsymbol{u}^k$:

$$J_{ij} \equiv \frac{\partial F_i}{\partial u_j} \tag{3.42}$$

After $\delta\boldsymbol{u}^{k+1}$ is calculated, the next value of the vector solution is:

$$\boldsymbol{u}^{k+1} = \boldsymbol{u}^k + \delta\boldsymbol{u}^{k+1} \tag{3.43}$$

In MOOSE, this Newton iteration is completed when the residual vector norm $|\boldsymbol{r}^k|$ or the relative residual vector norm between two iterations meet the convergence criteria imposed. The system of equations presented in equation (3.41) is a very large problem set. However, in the JFNK method, the Jacobian matrix does not need to be fully assembled as only the value of its action on a vector is required.

Strong preconditioning is required for Krylov methods to be efficient, or else the convergence is very slow. Using right precondioning as an example, equation (3.41) can be transformed to:

$$\boldsymbol{J}^k\boldsymbol{P}^{-1}\left(\boldsymbol{P}\delta\boldsymbol{u}^{k+1}\right) = -\boldsymbol{r}^k \tag{3.44}$$

where $\boldsymbol{P}$ is a preconditioning matrix. The precondtioning can be mathematical or physics based. Physics based precondtioning relies on removing terms in the system of equations that do not contribute much to the physics, whereas the mathematical preconditioning can use a variety of techniques including LU or iLU decomposition methods.

The PJFNK SPH method is very similar to the iterative SPH process; the SPH factors are applied in the same way to the cross sections but the values of the fluxes and SPH factors are updated at every residual evaluation instead of waiting for the complete solution to the diffusion or transport problem. This allows the correct, converged solution to be determined much faster as the time is spent actively geting closer to the solution instead of getting the exact solution of a linear problem which is used for the evaluation of new values between non-linear iterations. The PJFNK method is very robust as long as the initial condition

is within the radius of convergence of the Newton Method, and, for simple SPH problems, this is not an issue. However, for highly non-linear problems, such as those with very large reflector regions or void boundary conditions, the preconditioning might not place the initial condition within the radius of convergence of the Newton method. To circumvent this, a method was fashioned that uses the solution obtained after a few traditional SPH iterations as an initial condition to the PJFNK problem, which brings the problems within its radius of convergence. An important point to note about the use of the PJFNK SPH method is that instead of enforcing a convergence criteria between subsequent values of the SPH factors, the convergence criteria is applied to the linear and non-linear residuals of the fluxes. Since these values are usually very tight ($\epsilon < 10^{-8}$) and since the convergence of the SPH factors depends on the fluxes, the obtained solution is equivalent to the same convergence criteria imposed on the SPH iteration scheme, or better.

3.6 The Equation Schemes within MOOSE

In this section, the equations that are used to solve the neutron diffusion and transport equations within Rattlesnake are presented.

3.6.1 The Weak Form of the SPH Diffusion Equation

Since MOOSE is a finite element solver, one must properly write down the equations in a way that they can be solved by the FE method. This is done by writing the transport equations into the weak formulation. The derivation presented here is for the neutron diffusion equation.

The first step is to take the multigroup neutron diffusion equation (3.15) and apply the SPH factors to the cross sections. Then, this equation is multiplied by the test function ψ to obtain:

$$-\left(\nabla\cdot\mu_{m,g}D_{m,g}\nabla\phi_g\right)\psi+\mu_{m,g}\Sigma_{m,g}\phi_g\psi-\frac{\chi_g}{k_{eff}}\sum_{g'=1}^{G}\mu_{m,g'}\nu\Sigma_{f\,m,g'}\phi_{g'}\psi-\sum_{g'\neq g}^{G}\mu_{m,g'}\Sigma_{s,m}^{g\leftarrow g'}\phi_{g'}\psi=0 \tag{3.45}$$

Next, each term is integrated over the volume. We shall use the notation $(a,b)=\int_V a\cdot b dV$ to define the inner product and $<a,b>$ for surface integrals:

$$-\Big(\nabla\cdot\mu_{m,g}D_{m,g}\nabla\phi_g,\psi\Big)+\Big(\mu_{m,g}\Sigma_{m,g}\phi_g,\psi\Big)- \Big(\frac{\chi_g}{k_{eff}}\sum_{g'=1}^{G}\mu_{m,g'}\nu\Sigma_{f_{m,g'}}\phi_{g'},\psi\Big)-\Big(\sum_{g'\neq g}^{G}\mu_{m,g'}\Sigma_{s,m}^{g\leftarrow g'}\phi_{g'},\psi\Big)=0 \quad (3.46)$$

Integrating the first term by part and using Gauss's divergence theorem,

$$\int_\Omega \nabla\cdot\vec{g}dx=\int_{\partial\Omega}\vec{g}\cdot\hat{n}ds \quad (3.47)$$

to obtain:

$$\underbrace{\Big(\mu_{m,g}D_{m,g}\phi_g,\nabla\psi\Big)}_{Kernel}-\underbrace{\langle\mu_{m,g}D_{m,g}\nabla\phi_g\cdot\hat{n},\psi\rangle}_{Boundary\ Condition}+\underbrace{\Big(\mu_{m,g}\Sigma_{m,g}\phi_g,\psi\Big)}_{Kernel} \underbrace{-\Big(\frac{\chi_g}{k_{eff}}\sum_{g'=1}^{G}\mu_{m,g'}\nu\Sigma_{f_{m,g'}}\phi_{g'},\psi\Big)}_{Kernel}\underbrace{-\Big(\sum_{g'\neq g}^{G}\mu_{m,g'}\Sigma_{s,m}^{g\leftarrow g'}\phi_{g'},\psi\Big)}_{Kernel}=0 \quad (3.48)$$

To obtain the final SPH factors, MOOSE solves this equation for the unknown flux ϕ until convergence of the solution is met.

3.6.2 The SAAF Neutron Transport Equation

Rattlesnake was originally a radiation S_N transport application which was improved to allow other calculation schemes such as diffusion and spherical harmonics (P_N). In order to solve the SPH corrected transport equations, the Self-Adjoint Angular Flux (SAAF) formulation of the P_N and S_N equations was used in CFEM. This section goes through the SAAF transport equations followed by the derivation of the weak form of said equation.

In Section 3.4, the even and odd parity transport equations are used to derive the SPH corrected equation. Where one would normally solve the transport equations for the even and odd parirty equations, the SAAF method has the angular flux itself as an unknown. A simplified notation of the neutron transport equation is used from this point on, where instead of expanding the scattering and fission sources, we replace them by the symbols S and q respectively. As such, with the simplified notation, the neutron transport equation is:

$$\vec{\Omega} \cdot \vec{\nabla}\Psi + \Sigma^t \Psi = S\Psi + q \tag{3.49}$$

This equation is solved for Ψ:

$$\Psi = -(\Sigma^t - S)^{-1}\vec{\Omega} \cdot \vec{\nabla}\Psi + (\Sigma^t - S)^{-1} q \tag{3.50}$$

Equation (3.50) is substitued in the gradient term of equation (3.49):

$$-\vec{\Omega} \cdot \vec{\nabla}(\Sigma^t - S)^{-1}\vec{\Omega} \cdot \vec{\nabla}\Psi + (\Sigma^t - S)\Psi = q - \vec{\Omega} \cdot \vec{\nabla}(\Sigma^t - S)^{-1} q \tag{3.51}$$

Equation (3.51) is the SAAF neutron transport equation. It holds the same structure as the solved even and odd parity equations of the neutron transport equation. The derivation of the SPH correction is done with the even and odd parity equations instead of the SAAF equation since both methods are also equivalent.

To write the SAAF equation in its weak form, every term is multiplied by the test function ψ:

$$-\left(\vec{\Omega} \cdot \vec{\nabla}(\Sigma^t - S)^{-1}\vec{\Omega} \cdot \vec{\nabla}\Psi\right)\psi + (\Sigma^t - S)\Psi\psi = q\psi - \left(\vec{\Omega} \cdot \vec{\nabla}(\Sigma^t - S)^{-1} q\right)\psi \tag{3.52}$$

Integrating over the domain and applying the divergence theorem, the equation becomes:

$$\begin{aligned} \underbrace{\left(\vec{\Omega} \cdot \vec{\nabla}\Psi, (\Sigma^t - S)^{-1}\vec{\Omega} \cdot \vec{\nabla}\psi\right)}_{Kernel} + \underbrace{\left(\Psi, (\Sigma^t - S)\psi\right)}_{Kernel} - \underbrace{\langle \Psi, (\Sigma^t - S)^{-1}\vec{\Omega} \cdot \vec{\nabla}\psi\vec{\Omega} \cdot \hat{n}\rangle}_{Boundary\ Condition} = \\ \underbrace{\left(q, \psi\right)}_{Kernel} + \underbrace{\left(q, (\Sigma^t - S)^{-1}\vec{\Omega} \cdot \nabla\psi\right)}_{Kernel} - \underbrace{\langle q, (\Sigma^t - S)^{-1}\psi\vec{\Omega} \cdot \hat{n}\rangle}_{Boundary\ Condition} \end{aligned} \tag{3.53}$$

For the transport solver, whether is it through P_N or S_N, this is the weak form of the SAAF transport equation. The SPH correction is simply needed on each cross section, as defined in Section 3.4.

3.7 Observations and Issues with SPH

3.7.1 The Dependence of the Reference Eigenvalue on the SPH Equations

The SPH procedure requires some reference values from a lattice calculation: fluxes ϕ, cross sections Σ_x and eigenvalue k_{eff}. When the source problem is solved, an assumption is made that the reference eigenvalue is of great importance to the SPH procedure. However, this is not always the case. To illustrate this, the SPH corrected neutron diffusion equation is studied:

$$-\nabla\cdot\mu_{m,g}D_{m,g}\nabla\phi_g+\mu_{m,g}\Sigma_{m,g}\phi_g=\frac{\chi_g}{k_{eff}}\sum_{g'=1}^{G}\mu_{m,g'}\nu\Sigma_{f\,m,g'}\phi_{g'}+\sum_{g'\neq g}^{G}\mu_{m,g'}\Sigma_{s,m}^{g\leftarrow g'}\phi_{g'} \tag{3.54}$$

For reasons explained later, consider a problem where the scattering is negligible as opposed to the other physics involed, and as such can be ignored. The SPH equation to be solved is now:

$$-\nabla\cdot\mu_{m,g}D_{m,g}\nabla\phi_g+\mu_{m,g}\Sigma_{m,g}\phi_g=\frac{\chi_g}{k_{eff}}\sum_{g'=1}^{G}\mu_{m,g'}\nu\Sigma_{f\,m,g'}\phi_{g'} \tag{3.55}$$

Assuming the correct value of the reference k_{eff}, the fixed source equation is solved to obtain the flux $\phi^{correct}$ from which are calculated the SPH factors $\mu_{m,g}^{correct}$ using the Flux-Volume normalization scheme (equation 3.10). Using these values, the iterative scheme is continued until convergence is met.

Now, equation (3.55) is solved with an eigenvalue which is incorrect by a factor α, $k'_{eff}=k_{eff}\alpha$. The fixed source is now multiplied by $1/\alpha$ and the solution $\phi^{incorrect}$ is equal to $\phi^{correct}/\alpha$. We then calculate the SPH factors:

$$\mu_{m,g}^{incorrect}=\frac{\phi_{m,g}^{ref}}{\phi_{m,g}^{incorrect}}\frac{\bar{\phi}_g^{incorrect}}{\bar{\phi}_g^{ref}}=\frac{\alpha\phi_{m,g}^{ref}}{\phi_{m,g}^{correct}}\frac{\bar{\phi}_g^{correct}}{\alpha\bar{\phi}_g^{ref}}=\mu_{m,g}^{correct} \tag{3.56}$$

The previous equation shows that the SPH factors are the same whether or not the correct reference eigenvalue is used. For the next iterations, the same results are obtained: a wrong flux solution, but unchanged SPH factors. After the SPH iterations have converged, the values of μ are the same whether or not the eigenvalue was correct. This result is only applicable to problems with a very weak scattering contribution, such as 1 group diffusion since there is no scattering term. For problems where scattering is important, using the correct reference

eigenvalue is very important for the correct use of the SPH homogenization. Since this is an intrinsic result of the SPH procedure, it allows for a good test of the implementation of the method as it ensures conservation of the eigenvalue. This derivation also applies for the neutron transport equations.

3.7.2 Nonconvergence Issues

The SPH procedure has issues with reflector regions, which exhibit highly non-linear properties and prevent convergence of the solution (Ragusa et al., 2007; Pautz, 2006; Alain Hébert, 1981). This section goes through different attempts that were investigated to circumvent this problem.

Corrections for the Reflector Regions

Following the process explained by Pautz (2006), different SPH factors were defined for the reflector regions than for the rest of the problem. For regions which are not reflectors, the usual definition of the SPH factors is used with Flux-Volume normalization:

$$\mu_{m,g} = \frac{\phi^{ref}_{m,g}}{\phi_{m,g}} \frac{\bar{\phi}_g}{\bar{\phi}^{ref}_g} \tag{3.57}$$

For reflector regions, instead of normalizing the factors to preserve domain averaged fluxes, the fluxes at the fuel-reflector boundary were preserved, denoted as $\phi_{b,g}$:

$$\mu^{reflector}_{m,g} = \frac{\phi^{ref}_{m,g}}{\phi_{m,g}} \frac{\phi_{b,g}}{\phi^{ref}_{b,g}} \tag{3.58}$$

Another option is to force the conservation of the current at the fuel-reflector boundary $J_{b,g}$:

$$\mu^{reflector}_{m,g} = \frac{\phi^{ref}_{m,g}}{\phi_{m,g}} \frac{J_{b,g}}{J^{ref}_{b,g}} \tag{3.59}$$

The conserved current may be defined as the net, incoming or outgoing current. Pautz achieved convergence by doing these types of corrections on the reflectors but in our case these attempts proved unsuccessful. The correct implementation of this method was verified by comparing the values of the surface fluxes of currents at the fuel-reflector boundaries. Since the values obtained were identical to the reference values, it seemed that we could not converge to the correct solution which would also satisfy the added constraints. However, this was before the implementation of the PJFNK SPH method with free iterations; it may

still be possible that this type of correction works and we simply did not converge to the correct solution.

Condensing the Energy Groups

In the problems where convergence was impossible, we noticed the following trend; fluxes in the reflector regions for certain energy groups approach 0, always getting smaller and never meeting the convergence criteria. Since the flux contribution in those energy groups were small, we simply changed the energy group structure in a way that ensures that no fluxes approached 0 in any region. This was done by reducing the number of energy groups. In most cases, the fast groups were the cause of the problem and changing the group structure did not affect the physics of the problems. This opens the door for an adaptive condensation step to force the convergence of the problem.

PJFNK SPH

The application of MOOSE's PJFNK solver to the SPH non-linear problem was driven by the non-convergence issues. Since the PJFNK method is very robust as long as the initial condition lies within the radius of convergence of the Newton method, we had high hopes towards being able to solve the highly non-linear reflector problems, and this is the case. The use of the PJFNK SPH method with free SPH iterations allowed the convergence of problems that were not able to be solved with either the SPH iteration or PJFNK SPH. In other cases, the SPH iteration was shown to converge in problems containing large reflectors or void boundary conditions. This process was slow but the SPH method usually does not converge with these types of problems. This indicates that the SPH iterative procedure implemented within MAMMOTH is very robust since it relies on the PJFNK solver for the solution to the linear problems. However, with the use of the PJFNK SPH method, convergence was reached much faster, and also could generate results that were otherwise unobtainable.

CHAPTER 4 RESULTS AND DISCUSSION

4.1 Methodology

All reference solutions were obtained with the Monte Carlo Reactor Physics code Serpent2 (Leppänen, 2015) using ENDF/B-VII.1-based data. The generated homogenized cross sections were converted from the Serpent output to the YAKXS format with XSGEN, one of the MAMMOTH utilities. For all the problems tested with SPH, a 4 and 8 energy group structure from CASMO for Light Water Reactors (LWR) (Rhodes et al., 2006) were used as well as an 11 group structure which was derived from a 26 group High Temperature Reactor group structure (IAEA, 2003). These are found at tables 4.1, 4.2 and 4.3.

Table 4.1 4-Group structure, upper energy limits

4-group structure				
Group	1	2	3	4
$E_{\max}$ (MeV)	6.2500E-07	5.5300E-03	8.2100E-01	∞

Table 4.2 8-Group structure, upper energy limits

8-group structure				
Group	1	2	3	4
$E_{\max}$ (MeV)	5.5498E-08	1.3800E-07	2.7999E-07	6.2500E-07
Group	5	6	7	8
$E_{\max}$ (MeV)	4.0000E-06	5.0045E-03	7.0651E-01	∞

Table 4.3 11-Group structure, upper energy limits

11-group structure					
Group	1	2	3	4	5
$E_{\max}$ (MeV)	2.00100E-08	4.73020E-08	7.64970E-08	2.09610E-07	6.25000E-07
Group	6	7	8	9	10
$E_{\max}$ (MeV)	8.100030E-06	1.32700E-04	3.48110E-03	1.15620E-01	3.32870E+00
Group	11				
$E_{\max}$ (MeV)	∞				

To compare the results obtained through the SPH method with the reference heterogenous calculations, it is sensible to look at the error in power distribution. The error is calculated

with percent relative difference (%) as:

$$\epsilon = 100 * (\frac{Experiment - Reference}{Reference}) \tag{4.1}$$

from which is defined the "root-mean square" (RMS) error in power distribution :

$$\epsilon_{RMS} = \sqrt{\frac{\sum_m \epsilon_m^2}{\sum_m \neq 0}} \tag{4.2}$$

which represents the square root of the average of the square of the errors, where the sum in the denominator only counts non-zero values. In this section, the maximum and minimum errors are defined as the actual extrema, and not the extrema of the absolute values. This allows for a better observation of the total error range within a problem, defined as $\epsilon_{max} - \epsilon_{min}$.

4.2 Pressurized Water Reactor Assembly SPH Homogenization

The SPH method is known to work well with PWR assemblies and colorsets. As such, a set of simple problems to which the SPH method is usually applied was devised to test the implementation of said method. The first consisted of PWR assemblies, which are defined in the BEAVRS benchmark for a PWR (Horelik et al., 2013). Unless specified, the PJFNK SPH method was used to calculate these results.

These assemblies take the configuration of a 17x17 grid surrounded by a water gap and may include burnable absorbers, guide tubes, instrument tubes and control rods. The assemblies used in the analysis contain 3.1% enrichment fuel. For the testing of the SPH procedure, depending on the assembly type, we have homogenized our results down to approximately 10 to 15 regions. The grouping of these cells is based on the type of pin (fuel pin, burnable absorbers, control rods, etc.) and on their immediate neighbours. The symmetry of the problem is also taken into account during the homogenization process.

To obtain the reference values for the PWR assemblies, Serpent2 was used to model a high fidelity pin-by-pin continous infinite energy spectrum problem. Each fuel pin was modeled according to the BEAVRS benchmark specifications, including up to 6 different regions within each cell. The energy spectrum was then reduced to 8 energy groups and the homogenized cross sections were produced following the appropriate homogenization scheme.

Figure 4.1 shows the cell homogenization used for a 16 Burnable Pin assembly, where regions 15 represent the burnable absorbers, 13 denotes guide tubes, 12 a guide tube which may include an instrument tube and other regions represent fuel pins. A second assembly was

used to test the implementation of the SPH procedure; a control rod assembly that contains no burnable pins, and which was homogenized into 10 regions including the water gap, shown in Figure 4.2, where region 13 represents a control rod, 12 a guide tube with instrument tube and every other cell is fuel.

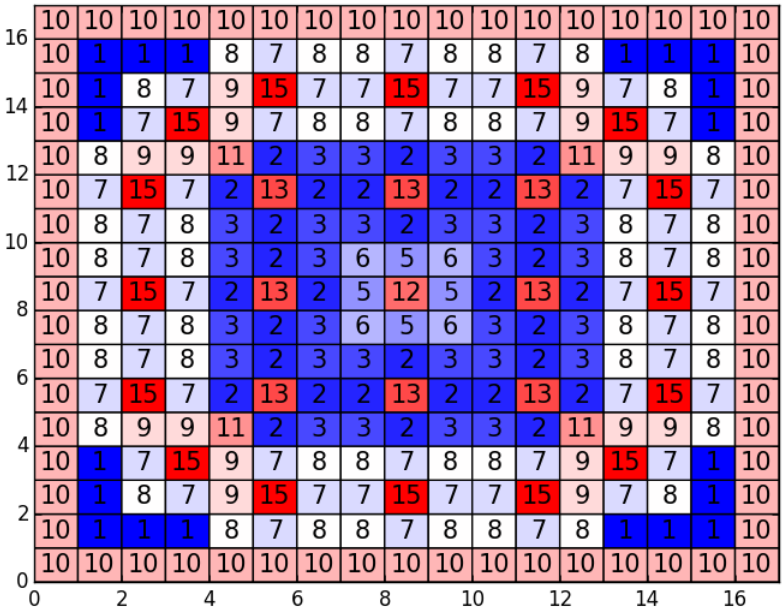

Figure 4.1 Cell homogenization scheme for a 17x17 PWR assembly that contains 16 burnable absorbers

4.2.1 Diffusion Results

The main goal of this thesis is to implement the SPH method for the diffusion equation for a continuous finite element method (CFEM). Results pertaining to the application of said method for the 16 burnable absorber assembly as well as the control rod assembly are shown here. Figures 4.3 to 4.6 show the error in the power distribution between the reference problem and the homogenized problem with and without SPH correction. A significant improvement is seen in both cases when the SPH correction is used; the RMS error is significantly reduced as are the maximum and minimum errors. The SPH corrected results seem to work better for the control rod assembly; this might be explained by the smoothing out of the effect of the control rods in the assembly by the homogenization. With SPH correction, the eigenvalue obtained is the same as the reference value (within 0.5pcm in both cases) whereas the non-SPH corrected cross sections reaches a difference of -11.8% for the control rod as-

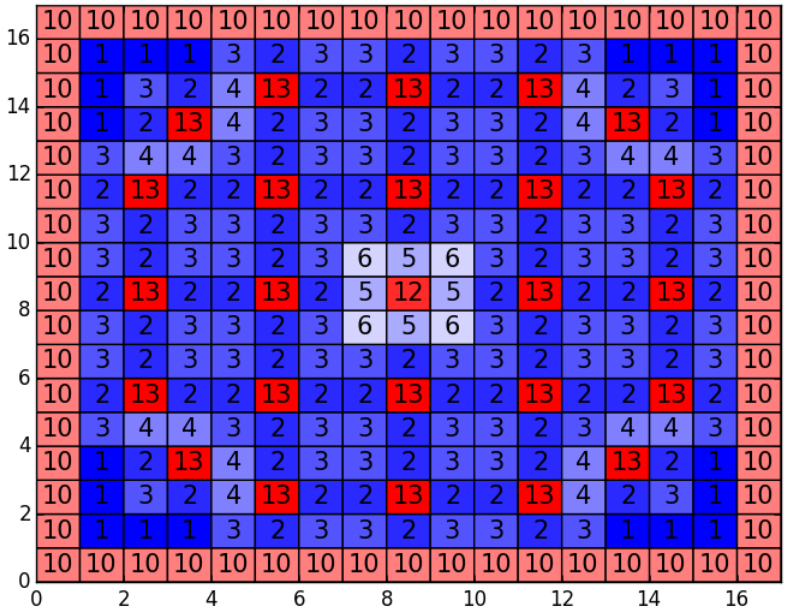

Figure 4.2 Cell homogenization scheme for a 17x17 PWR assembly that contains 24 control rods

sembly, as seen in table 4.4. We have not included figures showing the results obtained with the Selengut and true Selengut normalizations (equations (3.12) and (3.14)) since the power distributions are the same as with the flux-volume normalization (within the 3rd significant digit). These results indicate that the SPH correction to the diffusion equation seems to be well implemented and functional with PWR assemblies.

Table 4.4 k_{eff} for PWR assemblies in diffusion

	Reference k_{eff}	SPH $k_{eff}(\pm\%)$	NO SPH $k_{eff}(\pm\%)$
16BA Assembly	1.06051	1.06051 (0.00)	1.03584 (-2.33)
CR Assembly	0.817763	0.817764 (0.00)	0.721065 (-11.8)

4.2.2 Transport Results

The same cases are now studied with the transport SPH correction, using Rattlesnake's CFEM-SAAF-SN and CFEM-SAAF-PN methods combined with the PJFNK SPH procedure. To ensure high level of precision, the third order of the scattering matrix was used.

Figures 4.7 and 4.8 show the error in power distribution between the reference and the original

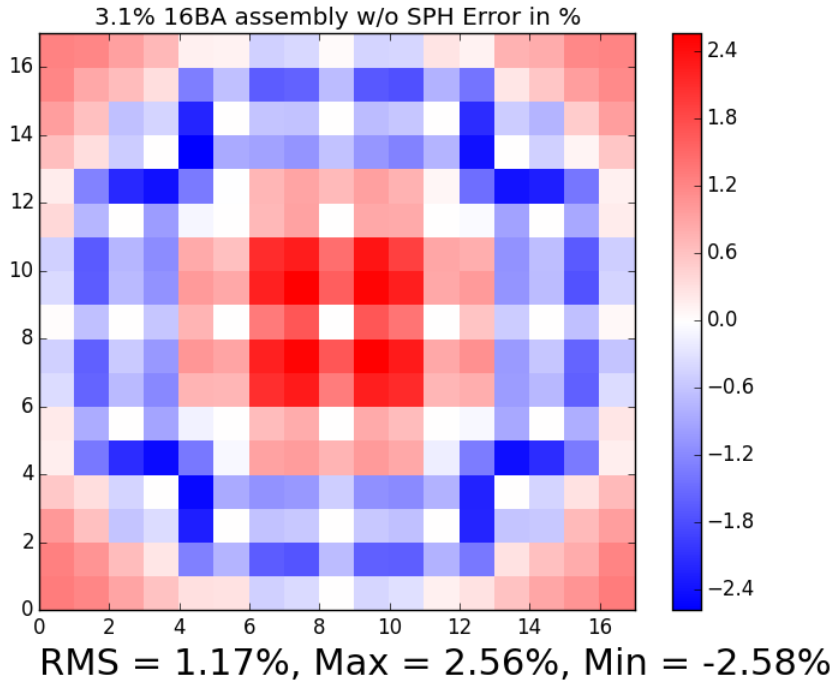

Figure 4.3 Error in power distribution for a 16 burnable absorber assembly without SPH for diffusion

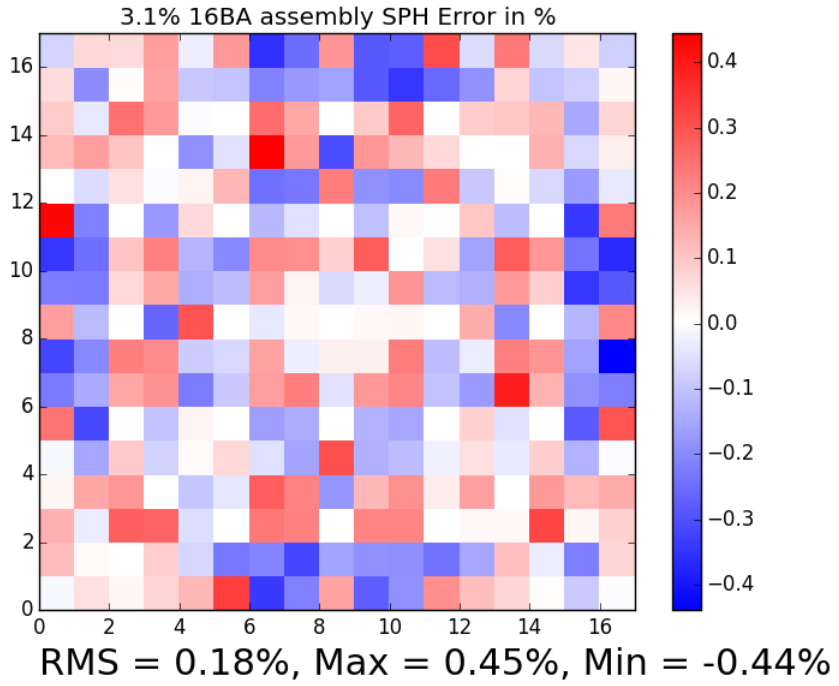

Figure 4.4 Error in power distribution for a 16 burnable absorber assembly with SPH for diffusion

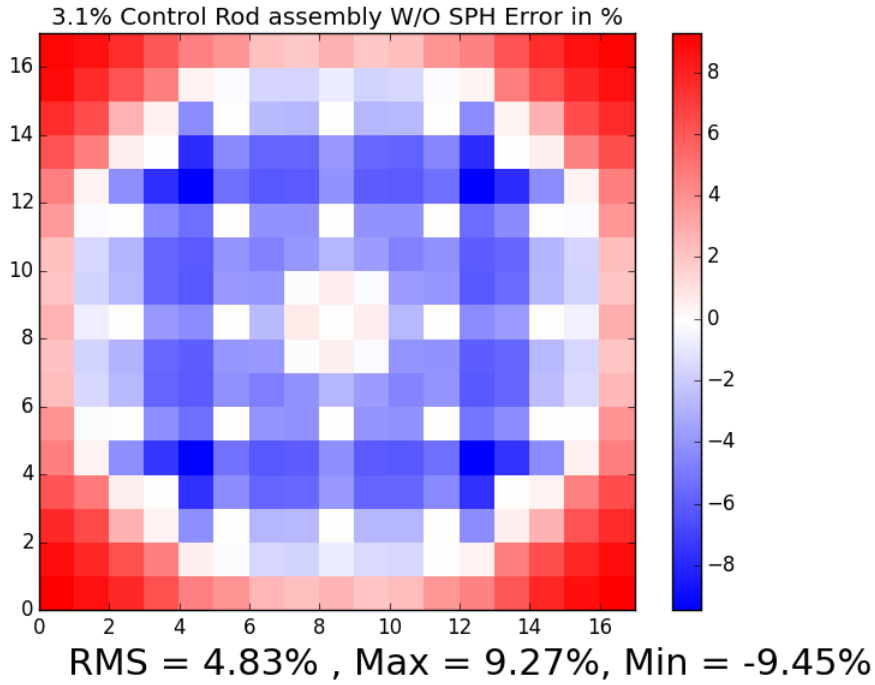

Figure 4.5 Error in power distribution for a control rod assembly without SPH for diffusion

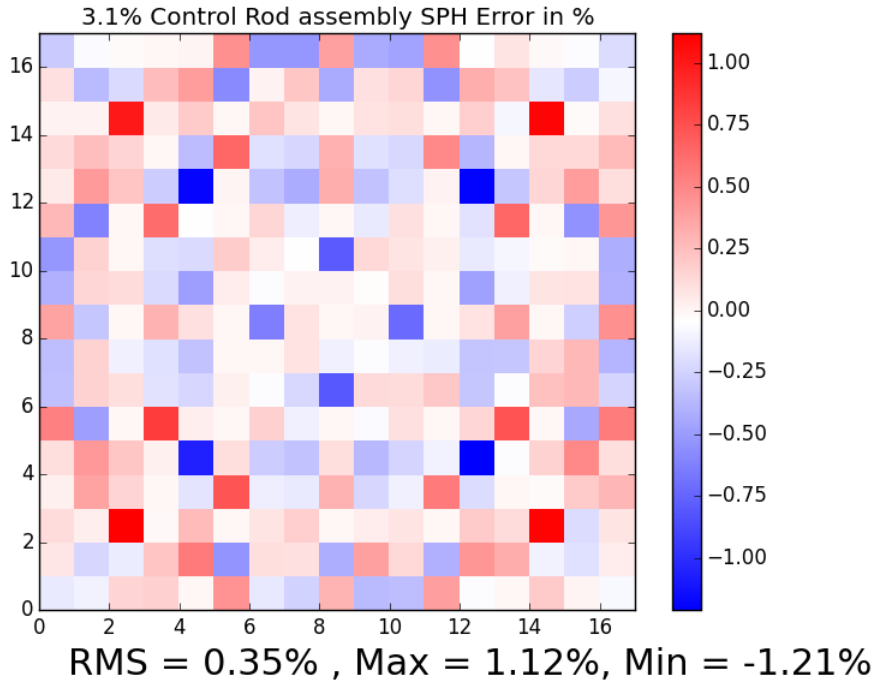

Figure 4.6 Error in power distribution for a control rod assembly with SPH for diffusion

cross sections and the SPH corrected ones, for a P_5 calculation for a control rod assembly. The RMS, maximum and minimum values of the error are reduced by a factor of 10 when the SPH correction is used. The error in power distribution is not included here with S_8 since both power distributions are nearly indistinguishable: the errors are the same within the 3rd significant digit.

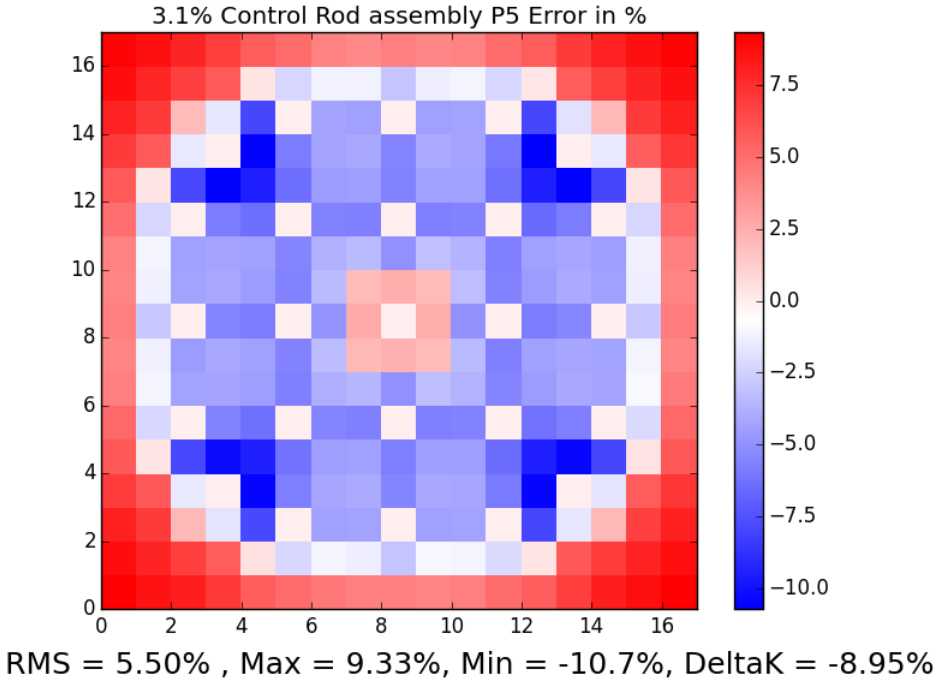

Figure 4.7 Error in power distribution for a control rod assembly without SPH for P_5

Table 4.5 k_{eff} for PWR assemblies for P_5

	Reference k_{eff}	SPH $k_{eff}(\pm\%)P_5$	NO SPH $k_{eff}(\pm\%)P_5$
16BA Assembly	1.06051	1.06051 (0.00)	1.0423 (-1.72)
CR Assembly	0.817763	0.817763 (0.00)	0.744575 (-8.95)

Figures 4.9 and 4.10 show error in power distribution for the 16 burnable absorber assembly calculated with S_8 with and without SPH correction. The improvements are quite significant: we reduce the RMS error by a factor of almost 10, and likewise with the maximum and minimum values of the error. The distinctive shape of the error is lost in the corrected case, showing that homogenization is done properly. Once again, the results obtained from the P_5 calculation to this assembly are not shown since they are too similar to S_8.

Tables 4.5 and 4.6 show the eigenvalue errors for both cases for the P_5 and S_8 schemes

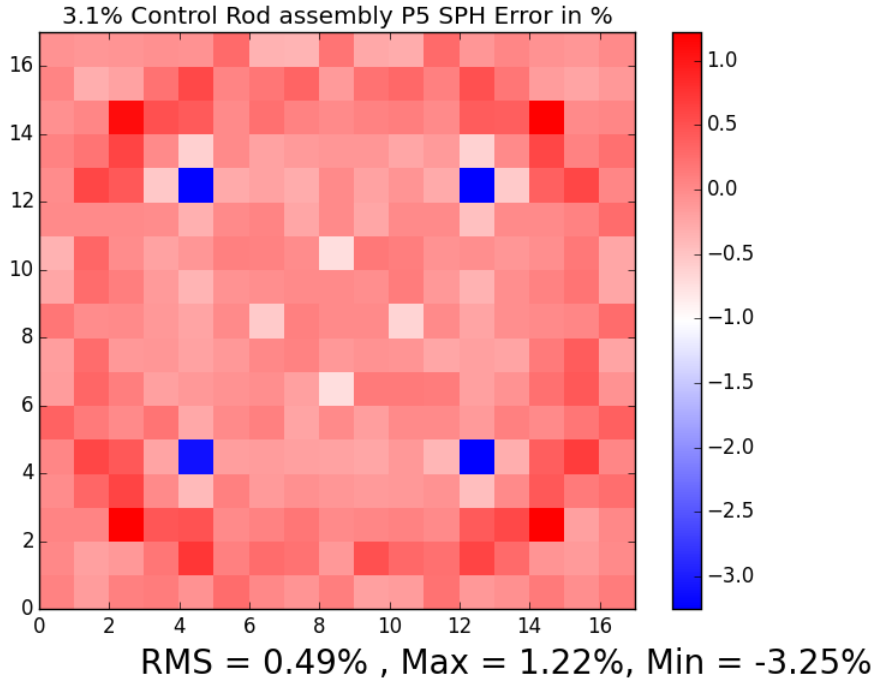

Figure 4.8 Error in power distribution for a control rod assembly with SPH for P_5

respectively. Without the use of the SPH correction, the 16 burnable absorber assembly shows an error of 1.73% on the eigenvalue and that value is down to exactly 0 when SPH correction is used with transport. The same result is observed for the control rod assembly: the error diminishes from 8.95% down to 0.

The SPH transport correction brings the errors to very small and similar values to those obtained through diffusion. The drastic improvements observed by using the SPH transport correction as well as the reproduction of the exact eigenvalue confirms the correct derivation and implementation of the transport SPH method.

Table 4.6 k_{eff} for PWR assemblies for S_8

	Reference k_{eff}	SPH $k_{eff}(\pm\%)S_8$	NO SPH $k_{eff}(\pm\%)S_8$
16BA Assembly	1.06051	1.06051 (0.00)	1.0423 (-1.72)
CR Assembly	0.817763	0.817762 (0.00)	0.74474 (-8.93)

4.3 2x2 Colorset Supercell Problem

The traditional use of SPH is to apply its correction on a smaller domain surrounded by reflective boundary conditions and using those cross sections in a larger domain calculation,

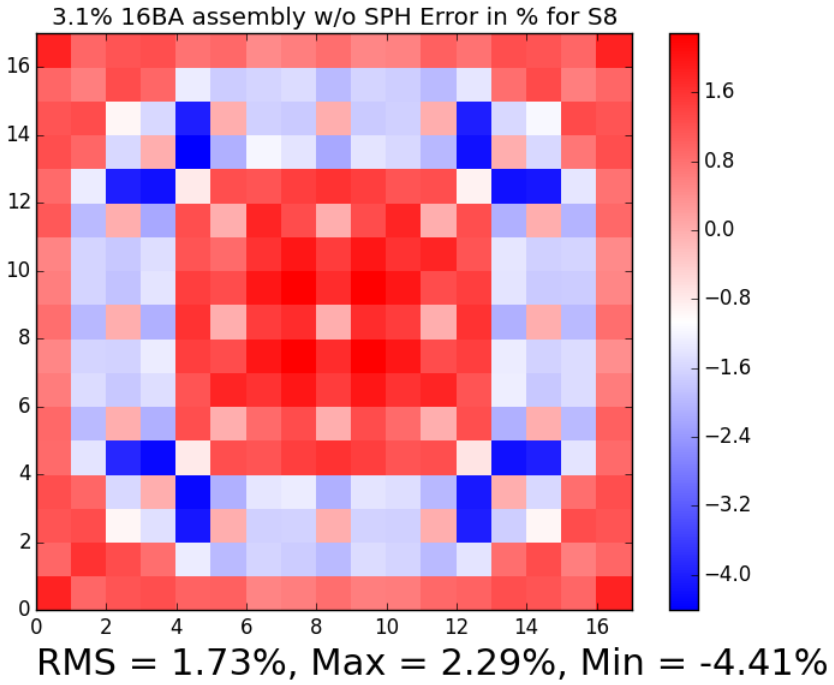

Figure 4.9 Error in power distribution for a 16BA assembly without SPH for S_8

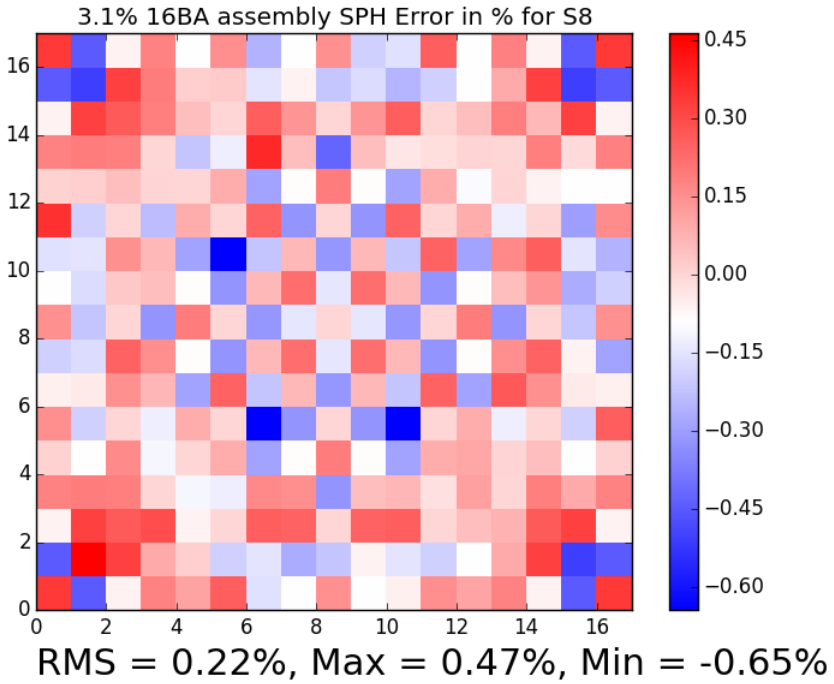

Figure 4.10 Error in power distribution for a 16BA assembly with SPH for S_8

such as a colorset of assemblies. In this section, results of a 2x2 colorset with a checkerboard pattern are shown. The colorset geometry is show in table 4.7, where assembly A stands for the 16 burnable absorber assembly shown in figure 4.1 and assembly B represents the control rod assembly at figure 4.2:

Table 4.7 2x2 Colorset pattern

A	B
B	A

The reference values for these colorset problems are obtained through a Serpent2 pin-by-pin calculation of the whole colorset.

4.3.1 Diffusion Results

Figures 4.11 and 4.12 represent the error distribution for the 2x2 colorset without and with the use of the SPH on the single assemblies with flux-volume normalization. We see a significant improvement in regards to RMS errors, and the range of errors when the SPH correction is used: the RMS error is reduced by a factor of 5, down to an almost acceptable level of 1.64% whereas the range of error decreases from 32% down to 7% . Table 4.8 shows the difference in eigenvalues from the reference and those obtained through single assembly homogenization. Once again, a clear reduction of almost a factor of 10 in error with SPH correction is observed. These kinds of results seem to indicate that the implementation of the diffusion SPH procedure has been done correctly within MOOSE.

Table 4.8 k_{eff} for the 2x2 colorset in diffusion

Reference k_{eff}	SPH $k_{eff}(\pm\%)$	NO SPH $k_{eff}(\pm\%)$
0.95639	0.95094 (-0.57)	0.90599 (-5.27)

4.3.2 Transport Results

We also compared the results of the 2x2 colorset obtained by solving the neutron transport equation with both P_5 and S_8 following the homogenization of the single assemblies. Figure 4.13 shows the error in power distribution when no SPH correction is applied to a P_5 solution. Figure 4.14 shows the error distribution with the SPH correction applied to the single assemblies through the neutron transport equation with P_5 with flux-volume normalization and figure 4.15 shows the errors when the true selengut normalization (equation 3.14) is applied.

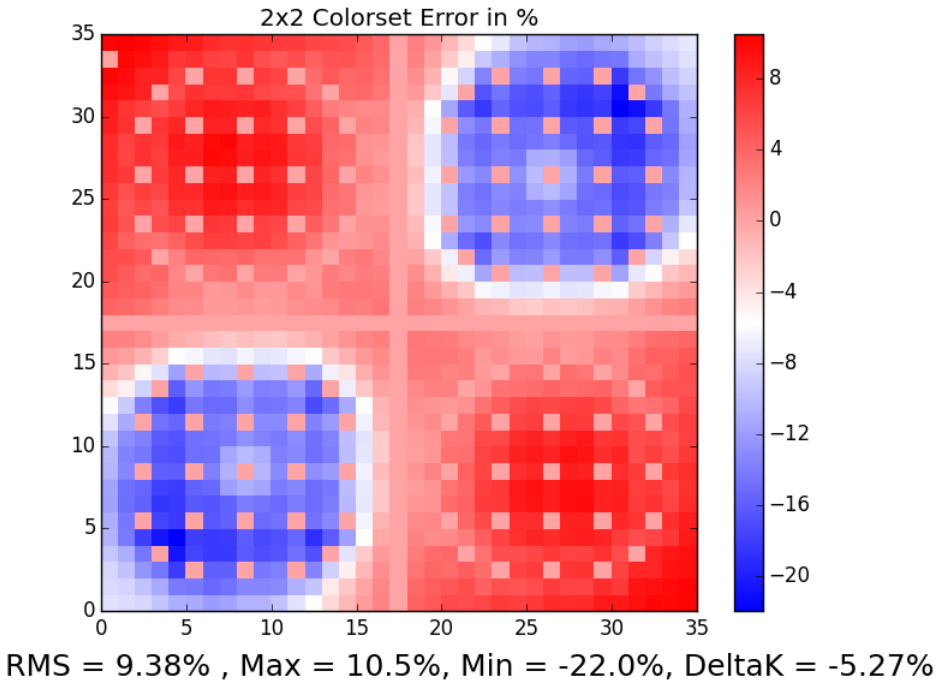

Figure 4.11 Error in power distribution for a 2x2 Colorset without SPH for diffusion

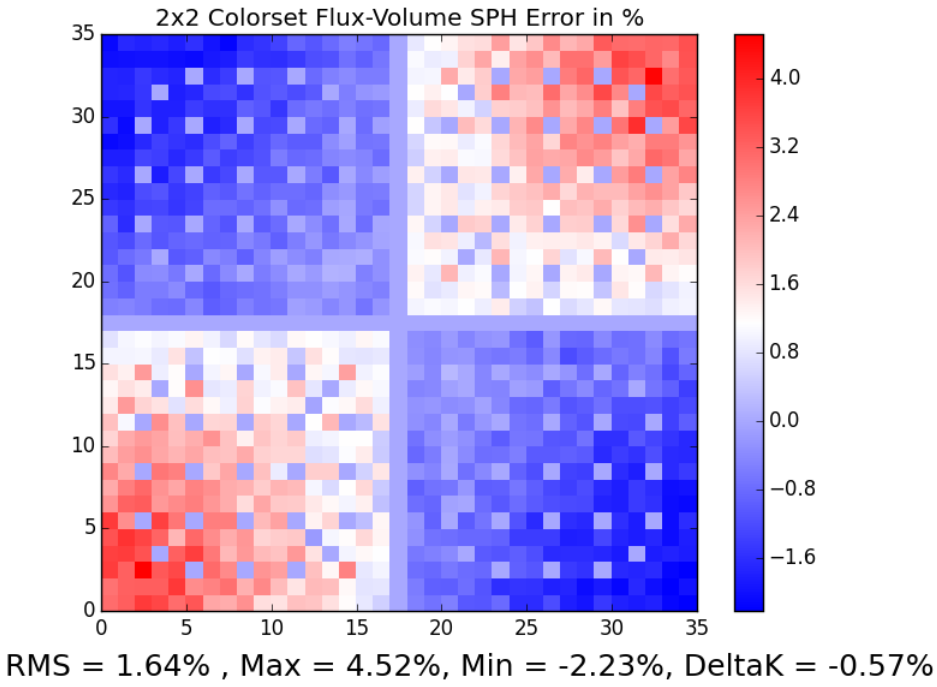

Figure 4.12 Error in power distribution for a 2x2 Colorset with SPH for diffusion and flux-volume normalization

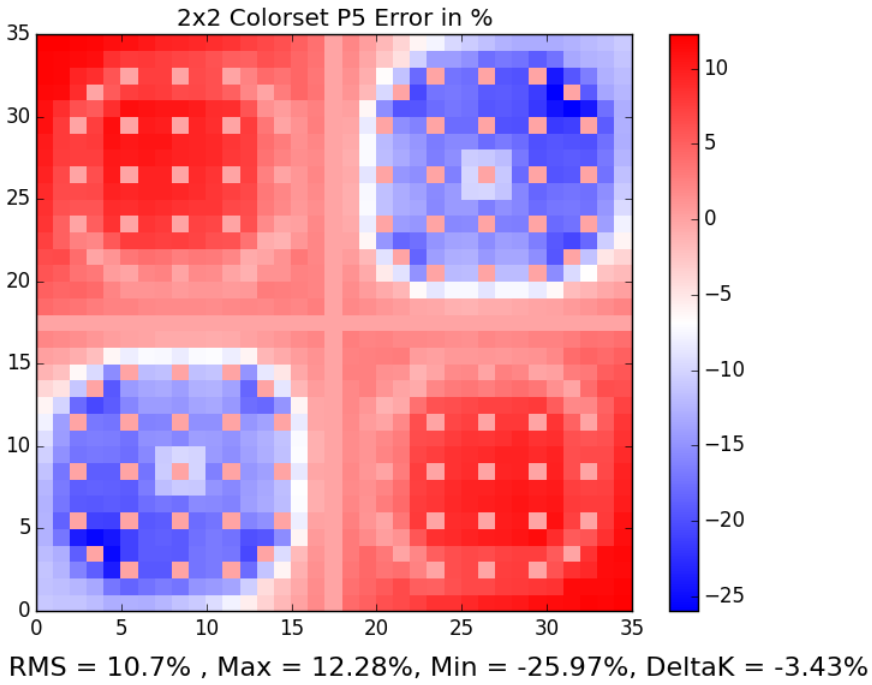

Figure 4.13 Error in power distribution for a 2x2 Colorset without SPH for P_5

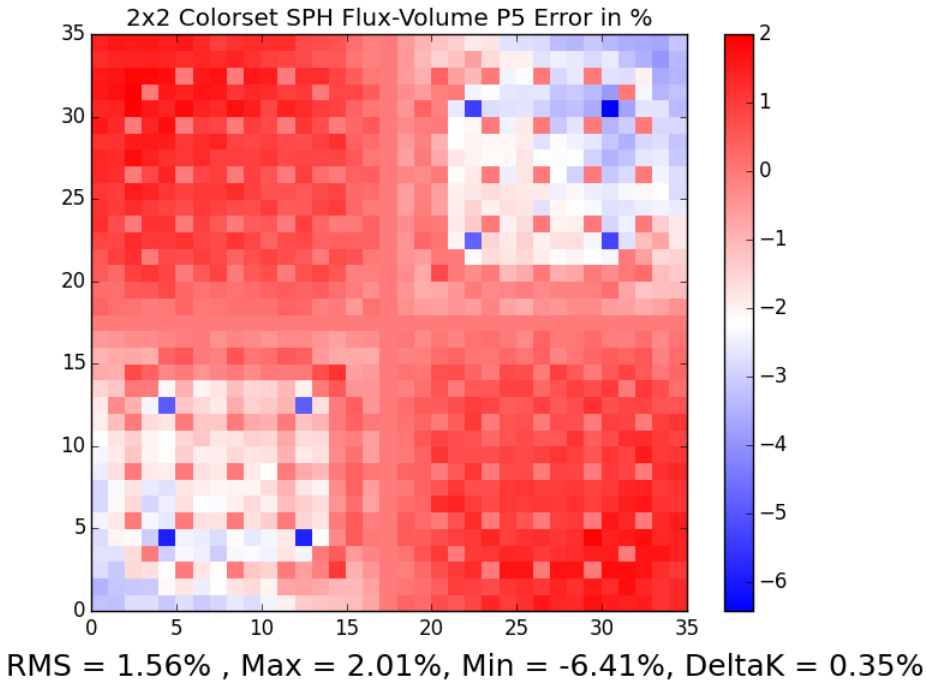

Figure 4.14 Error in power distribution for a 2x2 Colorset with SPH for P_5 and using flux-volume normalization

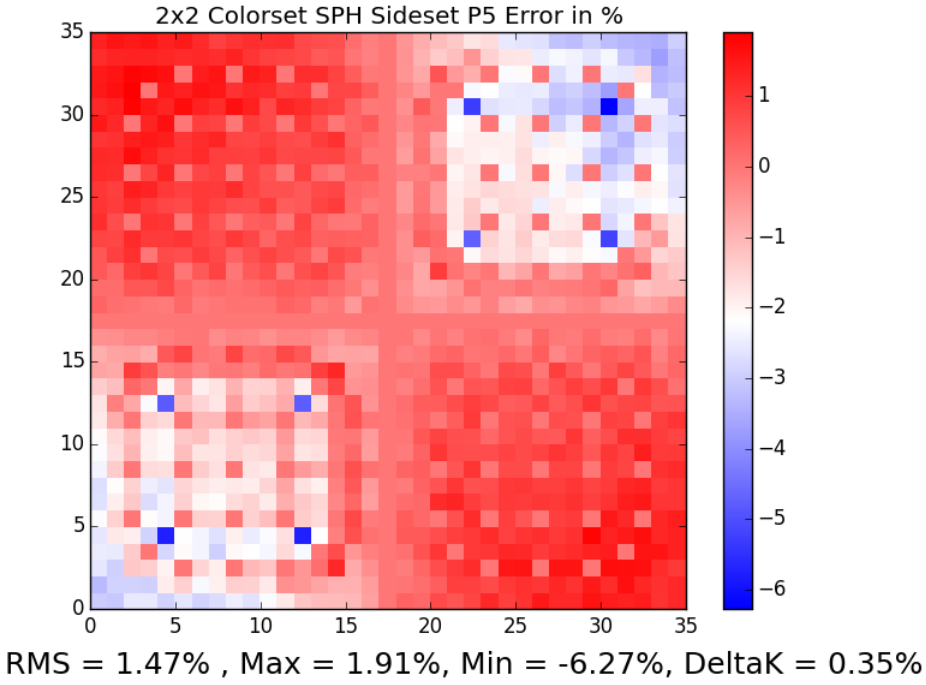

Figure 4.15 Error in power distribution for a 2x2 Colorset with SPH for P_5 and using true selengut normalization

Table 4.9 shows the eigenvalue of the colorset for the reference calculation as well as the uncorrected and SPH corrected cross sections.

Table 4.9 k_{eff} for the 2x2 colorset for P_5

Reference k_{eff}	SPH F-V $k_{eff}(\pm\%)$	SPH Selengut $k_{eff}(\pm\%)$	NO SPH $k_{eff}(\pm\%)$
0.95639	0.95974 (0.35)	0.95974 (0.35)	0.92359 (-3.43)

Once again, significant improvements are seen with the SPH corrected cross sections. We have not included figures of the results obtained with the S_N method since the results are the same (within the 3rd significant figure) as with the P_N method. The RMS error and error range is slightly reduced in the transport calculation when the true Selengut normalization is used as opposed to the Flux-Volume normalization. This agrees with the fact that the best results are expected to be obtained when using the Selengut type normalization. The power distributions and eigenvalues are also in better agreement with the reference values when we use transport SPH combined with the Selengut normalization than with the diffusion correction, although not by much. The minimum value on the error is found in fuel pins between control rods. This is either an interesting artifact, or we have not adequately homogenized our control

rod assemblies to account for transport effects. The transport SPH correction scheme does not produce significantly better results than the diffusion SPH correction in these PWR assembly problems. However, the results are very simliar. It is known that diffusion is extremely efficient and produces very good results with PWRs, and the fact that transport SPH produces the same results indicates that this method works. However, until transport SPH is tested on a problem that requires high order P_N or S_N calculations, there is no advantage using the SPH corrected transport over diffusion.

4.4 Notes on the SPH Functionality

4.4.1 Effect of Mesh Refinement

A study of the effect of the mesh on the SPH factors was also conducted for the PWR assemblies. MOOSE directly allowed us to refine our mesh for our problem no matter the transport scheme, allowing us to quadruple the number of elements used in our calculation (for quadratic elements). Figure 4.16 shows the effects of mesh refinement within MOOSE. The default mesh refinement value is level 0 which is no refinement. In 2D, a mesh refinement of level 1 creates four "children" elements when using quadratic elements. Each increasing level performs the same refinement on each of the previous' children elements.

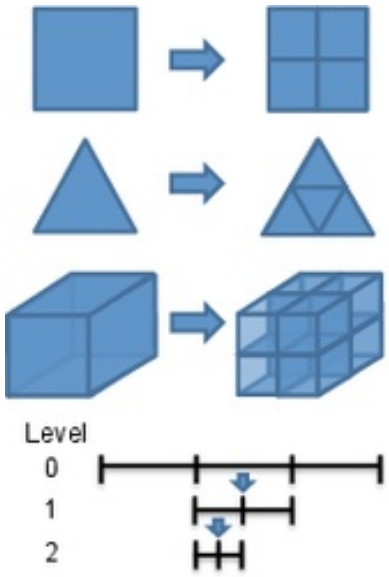

Figure 4.16 Mesh Refinement within MOOSE. Image taken from http://mooseframework.com/wiki/MooseTraining/Adaptivity/

This allows us to easily calculate the SPH factors for different mesh refinements. However, an issue arose when attempts were made to compute the power distributions with mesh

refinement and the idea had to be dropped. This limits our capabilities of studying the full effects of mesh refinement, but we may still look at the way the SPH factors behave as we refine the mesh.

Figure 4.17 shows the values of the SPH factors depending on the mesh refinement selected for the control rod assembly. This problem was homogenized to 10 regions and 8 energy groups. The SPH factors are defined in increasing order with the fuel pin numbers, going from energy group 1 to 8. As such, the first 8 SPH factors are those of fuel pin 1, for all 8 energy groups, followed by the 8 following factors for fuel pin 2. As the mesh is refined, the SPH factors move closer and closer to 1, without exception. A seemingly weird behaviour is also observed; a severe dip in the values of the SPH factors within a region. The region that contains the SPH factors that approach 0.6 is the control rod region. At first glance, this might seem wrong but although we may not calculate the power distribution, we still obtain the eigenvalue for the problem, which for all 3 cases, are exactly equal to the reference value. This indicates that the reaction rate is conserved no matter the mesh, but that we actually soften the flux shape within the problem. These results seem coherent with the fact that refining the mesh produces results that are a better representation of the actual solution.

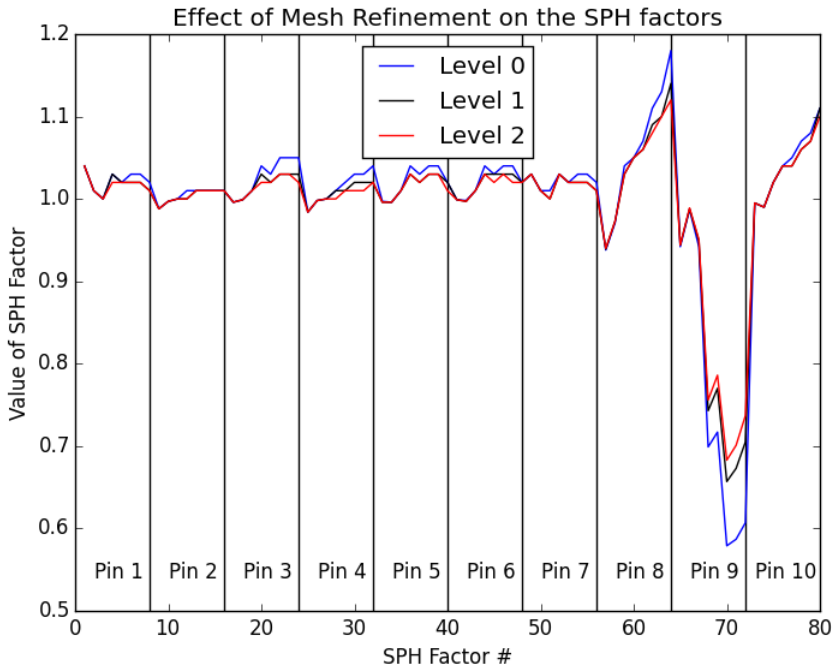

Figure 4.17 Effect of Mesh refinement on the SPH factors on the Control Rod Assembly

4.4.2 PJFNK SPH

The combination of the PJNK solver with the SPH method was implemented for the first time in this research project. As such, an extra step is needed to verify that both the traditional SPH iteration and SPH PJFNK methods produce the same results. Table 4.10 shows the maximum relative difference between the PJFNK obtained SPH factors and those obtained through the SPH iterations. These simulations were performed for a PWR control rod assembly. Table 4.10 shows that the relative difference between the PJFNK and iterative SPH factors are of the same order of magnitude as the convergence criteria imposed on the iterative scheme. Indeed, as the convergence criteria is tightened, the maximum difference in SPH factors goes to the same value. This indicates that the SPH factors obtained through the PJFNK method are the exact values whereas the iterative SPH scheme brings us towards that value. This is because the PJFNK method sets its convergence criteria on the evaluation of the residual of the fluxes, and this value is very tight. Therefore, both the flux solution and SPH factors are very tightly converged. Not only does the PJFNK method give us the most correct values of the SPH factors, but it does so in a much faster manner. The calculation time required for the PJFNK solver was 10 times smaller than that of the loosest convergence criteria imposed on the SPH iteration (10^{-4}). Of course, these results only hold true when the initial condition of the PJFNK solver is within the radius of convergence of the Newton method, as convergence is unattainable if we are outside said radius.

Table 4.10 Maximum Relative Difference in SPH factors. Difference calculated as $\frac{Iteration-PJFNK}{PJFNK}$. CPU time for PJFNK was 2.5 seconds.

	$\epsilon = 10^{-4}$	$\epsilon = 10^{-6}$	$\epsilon = 10^{-8}$
Largest relative difference in SPH factors	2.80E-04	2.71E-06	2.93E-08
CPU time in secs (# of iterations)	22 (36)	38 (69)	50 (101)

For problems smaller in size such as single assemblies, the PJFNK SPH shows its strength when solving the transport equation. Indeed, for a P_5 calculation of the control rod assembly, the SPH iteration scheme takes on average 818 seconds to achieve a converged solution for $\epsilon = 10^{-4}$ while the PJFNK method allows for the same problem to be solved in only 9.4 seconds, a reduction of a factor of nearly 100.

4.4.3 Effects of the P_N and S_N order

An interesting question arises about the effects of the order of the polynomial expansion P_N or the discretization order S_N on the SPH method. As such, using the transport SPH equations, we have studied how the RMS error behaves as we increase the order of our calculation.

Figure 4.18 shows the variation in the RMS errors in power distribution obtained through a control rod assembly when increasing the order of expansion N. The RMS error decreases as expected but stops reducing significantly quite rapidly when using P_5 and S_8. This is not the case when we do not use the SPH correction, where the RMS error continually gets smaller at the cost of much higher computation time. This confirms the assumption taken that the SPH correction should concentrate on the contributions to the reaction rate from the first few orders of the flux expansion. Using P_5, we also studied the effects of the contribution of the scattering order to the SPH transport correction. Table 4.11 shows the RMS error in power distribution for a control rod assembly corrected with SPH for the P_5 equations. Although the reference eigenvalue was always exactly reproduced, we find a drastic improvement in the power distribution when we consider the first scattering order contribution in our equations, but no improvement when considering the second. This should be studied in more detail for problems where scattering is highy anisotropic. Following these results, we have used the first 3 scattering orders in every calculation involving SPH transport.

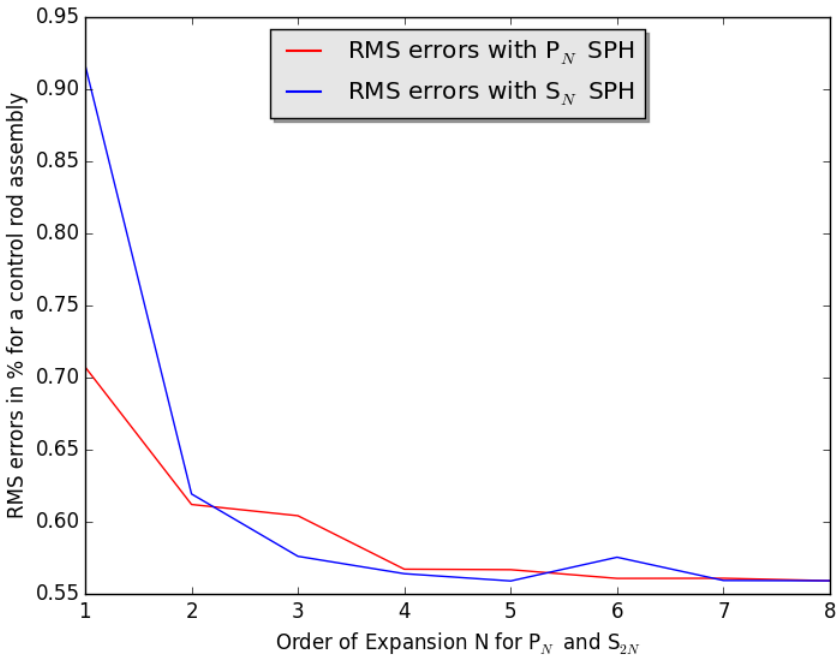

Figure 4.18 Effect of the order of N in the P_N and S_{2N} on the SPH transport correction

4.4.4 Σ^t Correction

We mentioned previously (Section (3.4)) that the total cross section can be corrected in two different manners. Figures 4.8 (in Section 4.3.2) and 4.19 show the power distribution error

Table 4.11 RMS error as a function of the scattering order for a P_5 SPH Correction

Angular flux moment	0	1	2
RMS error (in %)	2.43	0.57	0.58

obtained when the total cross section is corrected and not corrected in a control rod assembly problem for a P_5 calculation. A slight improvement is noticeable on the absolute values of the errors as well as a reduction of the RMS error when the total cross section is corrected. However, in the 16 burnable absorber assembly, we see no significant (smaller than 0.01%) difference between the two correction schemes. We have not found a reason as to why the power distributions may or may not differ according to the correction scheme, as both are mathematically equivalent assuming a high enough expansion order N. The same behaviour is observed for a S_N calculation.

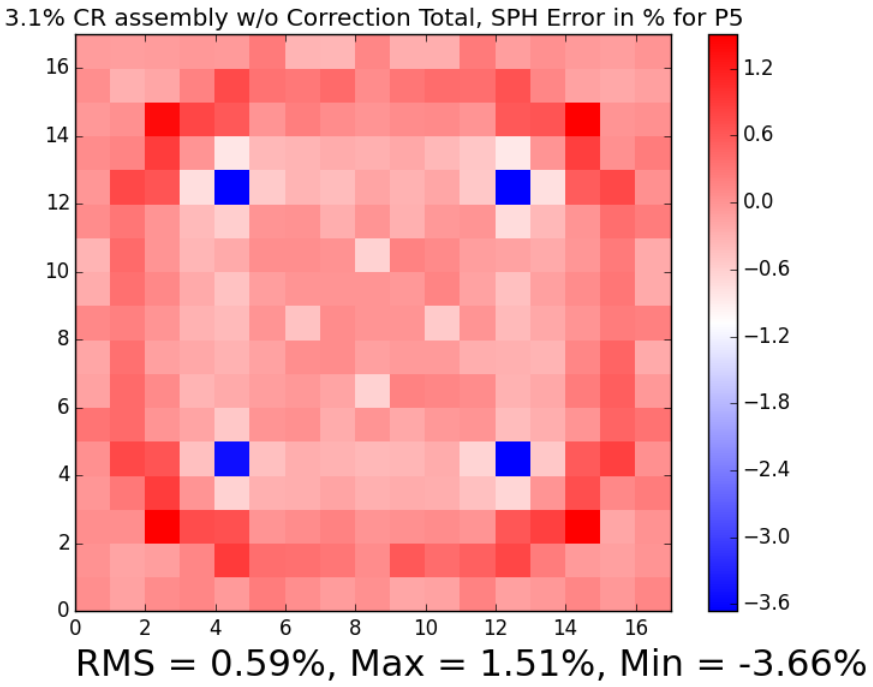

Figure 4.19 Error in power distribution for a control rod assembly with SPH without modification of the total cross section for P_5

4.5 Simplified Model of a PWR Including Water Reflectors

To have a better idea of the efficiency of the PJFNK SPH method, a simplified model of a PWR was considered from the BEAVRS benchmark (Horelik et al., 2013). This problem

represents the full line of 15 fuel assemblies passing through the centre core of the PWR, the water reflectors and the baffle. The general geometry of the problem is shown in Table 4.12, where we grouped the assemblies to be homogenized together by numbers and where "fuel" represents a fuel assembly, "baffle" represents the baffle, "water" is the water reflector and "6BA", "12BA" and "16BA" represent 6 , 12 and 16 burnable absorber assemblies respectively. The problem is symmetric, and as such we have illustrated only half the geometry. The problem has reflective boundary conditions on the top and bottom and vacuum boundary conditions on the left and right edges. Each assembly is homogenized to between 10 to 15 regions each, totalling 112 regions including the water gaps, baffle and water regions. The SPH procedure was applied to the diffusion equation with the flux-volume normalization.

Table 4.12 Half-Geometry of the Simplified PWR model

Assembly ID	1	2	3	4	5	6	7	8	9	10
Assembly material	water	baffle	6BA	fuel	16BA	fuel	12BA	fuel	16BA	fuel

The full SPH correction of this problem, with the help of the PJFNK method, only took 291 seconds on average. In contrast, the SPH iterative method took on average 5681 seconds to solve 355 iterations to reach its convergence criteria of $\epsilon = 10^{-4}$. This represents a reduction in calculation time of a factor of almost 20. Since the traditional SPH method has been known to not reach convergence in reflector and vacuum boundary problems, the fact that this problem has converged with the SPH iteration is interesting. It would seem that since the SPH iterative scheme also relies on the PJFNK method to obtain a solution of the linear problem at each iteration, we have created a more robust SPH iterative method. This goes to show that the PJFNK method allows for a very robust implementation of the SPH method. Table 4.13 shows the differences in eigenvalues obtained without and with the SPH correction. A drastic improvement is seen, from an error of 1.2% to within 0.06% when SPH is used. Since this is not a fully reflective boundary conditions, we cannot perfectly reproduce the eigenvalue.

Table 4.13 Values of the k_{eff} for the simplified PWR problem

Reference k_{eff}	Without SPH $k_{eff}(\pm\%)$	With SPH $k_{eff}(\pm\%)$
0.991575	0.979242 (-1.244)	0.990995 (-0.058)

The error in power distribution for the whole problem is shown at table 4.14. Once again, there is a drastic improvement with the use of SPH. The RMS error is less than a quarter of a percent, which is largely adequate when it comes to the modelling of nuclear reactors. The total range in errors is also greatly reduced. Even better results could be obtained by

creating more regions within the assemblies to take into account the flux shape variations within the full problem whenever a higher precision is needed. The value of the RMS errors for each individual assembly in this problem closely resembles the domain averaged values. This means that every assembly lies within an RMS error between 0.9 and 0.26 percent with the use of the SPH method. This not only shows that the SPH method works with vacuum boundaries and reflectors, it also conserves the power distribution quite well in every region of the reactor. Of course, this is not a full PWR test so no assumptions can be made to say that the SPH method captures all the properties of the reflectors.

Table 4.14 Errors in power distribution for the whole PWR problem

SPH?	RMS in %	Maximum Error in %	Minimum Error in %
Yes	0.179	0.927	-0.783
No	3.71	5.02	-10.3

Another test that consisted in homogenizing each singly assembly and using those cross sections to model this same problem was attempted. However, the RMS error obtained was around 3% for both the cases with and without the use of the SPH corrected cross sections. This is also true when using SPH with Selengut normalization. The SPH method is usually able to improve results for these kinds of problems, and we are unsure as to why we do not see an improvement for this situation.

4.6 Simplified TREAT Model Homogenization

A simplified model of the INL's TREAT reactor was also analysed using cross sections corrected by the SPH procedure (Ortensi et al., 2016). All the figures and data presented in this section originate from (Ortensi et al., 2016). The model consists of a 3x3 supercell with a central control rod, surrounded on the z axis by large regions of graphite reflectors and vacuum boundaries. The Serpent2 geometry is shown in figure 4.20 and an axial cut of the problem is shown in figure 4.21.

The SPH procedure was applied to this problem using the corrected neutron diffusion equation. However, convergence was not reached with the PJFNK SPH method. This problem was circumvented by employing "Free SPH iterations" before the PJFNK method to allow the initial condition to be within the radius of convergence of the Newton method. These "Free SPH Iterations" are performed using unconverged results from a SPH iterative solution with a small number of iterations. These results are then used as initial solutions for the PJFNK solver. In this case, 5 Free SPH iterations were used. Table 4.15 shows the average

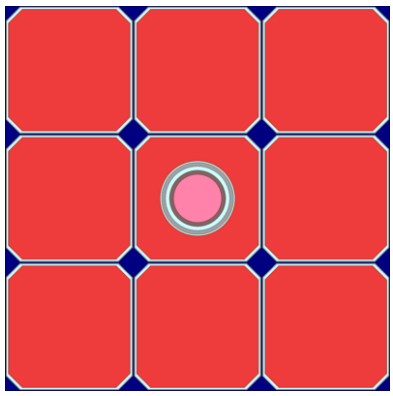

Figure 4.20 Geometry of the 3x3 supercell generated by Serpent2

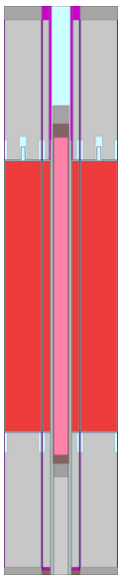

Figure 4.21 Axial representation of the 3x3 supercell, showing the control rod region. The grey regions are reflectors.

CPU time and number of free iterations needed for convergence. It is interesting to note that for both the 4 and 11 group cases, the SPH iteration reached convergence, albeit with a loose convergence criteria. The SPH method does not converge when reflector regions are present, however this is not what is observed here. Our SPH method relies on the PJFNK algorithm to solve the linear iterations, and this might be the cause of our convergence. However, for the PJFNK SPH method to work we needed 3 and 5 Free SPH Iterations for the 4 and 11 groups problem respectively. Increasing the number of Free SPH iterations did not necessarily decrease overall computational time, and more study on this behaviour is needed. Although the SPH iterations did converge, they took as much as 45 times the amount of time that the PJFNK SPH method required.

Table 4.15 SPH calculation parameters with inserted control rod for the simplified TREAT model

Solve Type	Energy Groups	Free SPH iterations	Average CPU time in secs
SPH iteration	4	-	660.0
PJFNK SPH	4	3	60.7
SPH iteration	11	-	9280
PJFNK SPH	11	5	202.9

Tables 4.16 and 4.17 show the difference in eigenvalue, fission, absorption and leakage rates for the 4 and 11 energy group problem. An important improvement is seen when the SPH method is used in eigenvalue for both the 4 and 11 energy group problems, with control rods inserted or not. The fission, absorption and leakage rate errors are also all reduced. Although a very large error in terms of the leakage rate is observed, which is caused by the vacuum boundary condition, this does not create a very large error in the eigenvalue since the leakage rates are orders of magnitude smaller than absorption and fission rates.

Table 4.16 Results for the 3x3 Supercell model for Diffusion with 4 groups

Control Rod	SPH?	k_eff difference (pcm)	Fission rate difference (%)	absorption rate difference (%	Leakage rate difference (%
Withdrawn	No	850.7	-0.851	-0.418	-25.438
Withdrawn	Yes	287.7	-0.295	-0.012	-16.307
Inserted	No	-6297	6.029	6.663	-20.174
Inserted	Yes	378.4	-0.415	-0.093	-13.653

Figures 4.22 and 4.23 show the axially averaged radial power distribution (ARPD) error for the 4 group problem, without and with SPH correction, while figures 4.24 and 4.25 show the same information for the 11 group problem. As expected, the 11 group problems exhibit

Table 4.17 Results for the 3x3 Supercell model for diffusion with 11 groups

Control Rod	SPH?	k_eff difference (pcm)	Fission rate difference (%)	absorption rate difference (%	Leakage rate difference (%
Withdrawn	No	1028.4	-1.025	-0.494	-31.273
Withdrawn	Yes	289.3	-0.296	0.006	-17.383
Inserted	No	-6297	7.406	6.708	-22.149
Inserted	Yes	378.4	-0.062	-0.389	-13.851

better results than those with 4 groups. This does not mean that the SPH corrected 4 group problem produces bad results, as the RMS error is still smaller than 0.7%, twice as large as the value of the 11 group solution. The ARPD error is significantly reduced between the SPH non-corrected and the corrected results. This and the PWR assembly line described above in Section 4.5 seem to show that this novel implementation of the SPH procedure may be able to correct actual, full reactor cores that contain large reflector regions and vacuum boundary conditions.

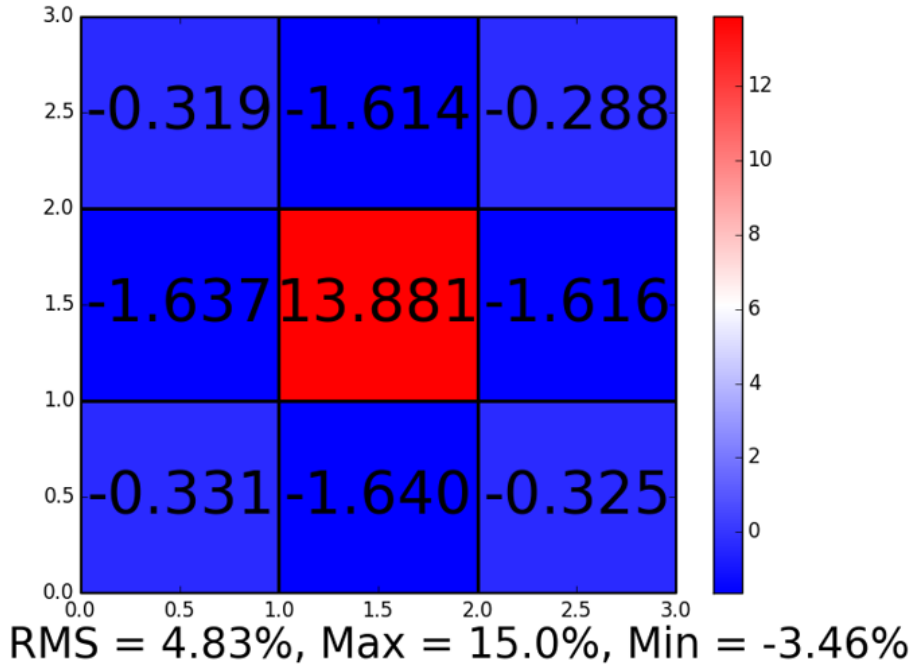

Figure 4.22 ARPD for the 4 group 3x3 supercell problem with diffusion.

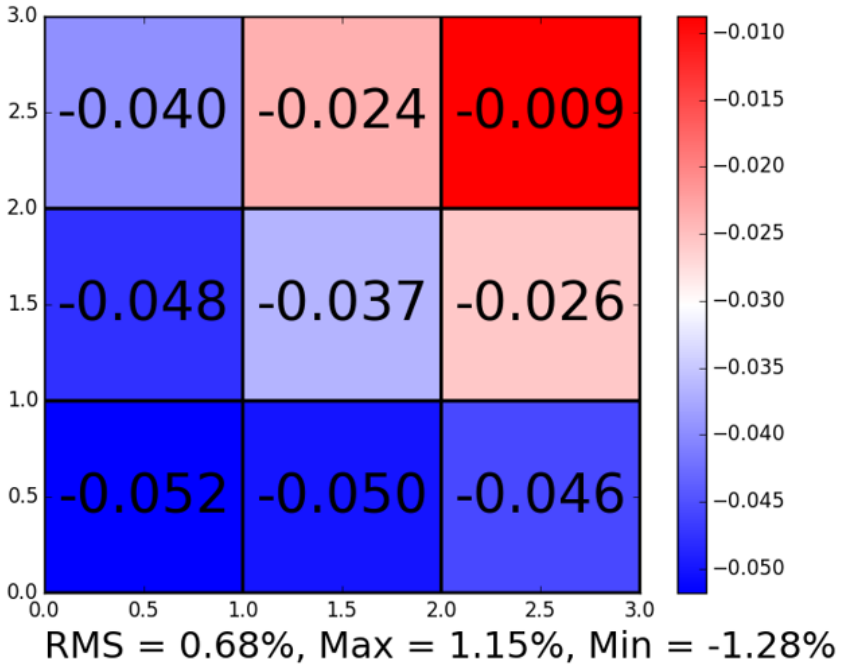

Figure 4.23 ARPD for the 4 group SPH corrected 3x3 supercell problem with diffusion.

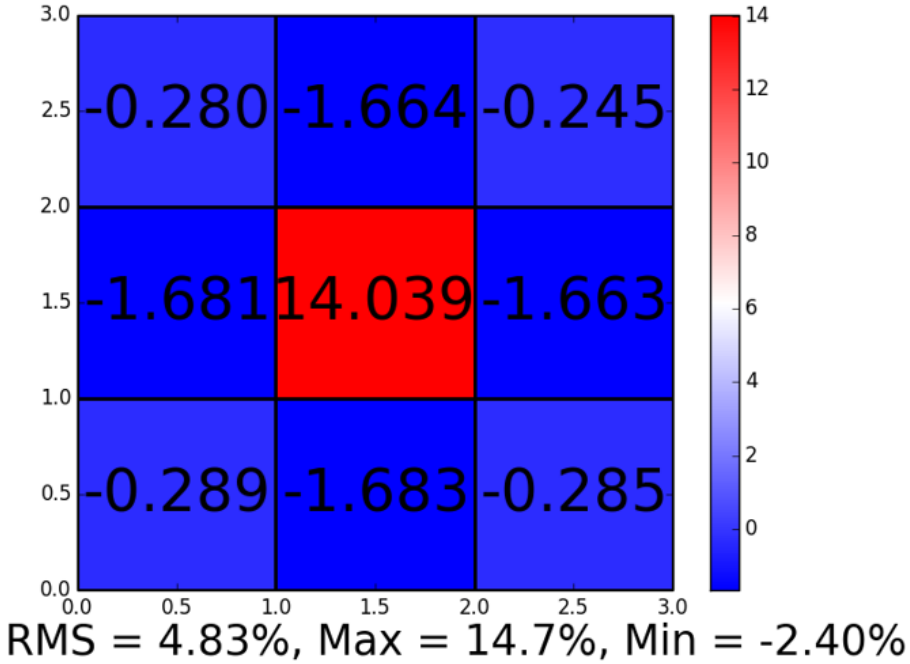

Figure 4.24 ARPD for the 11 group 3x3 supercell problem with diffusion.

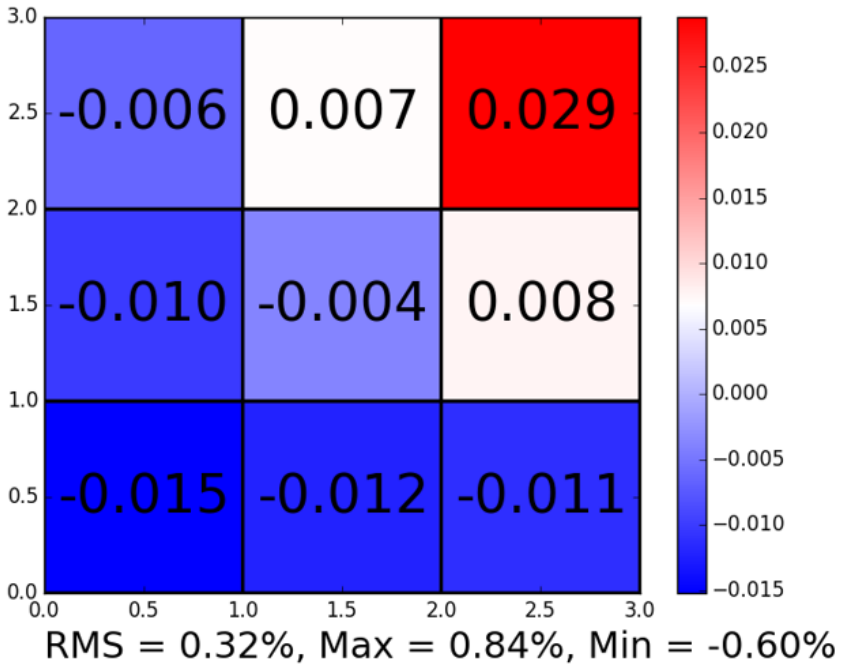

Figure 4.25 ARPD for the 11 group SPH corrected 3x3 supercell problem with diffusion.

CHAPTER 5 CONCLUSION

5.1 Synthesis of the Work

The Superhomogénéisation (SPH) method was successfully implemented within the MAMMOTH application at Idaho National Laboratory. Using the neutron diffusion equation as well as the even and odd parity equations of the neutron transport equation, the SPH procedure was derived for the diffusion and transport equations. The SPH corrected CFEM diffusion and SAAF S_N and P_N equations were tested on PWR assemblies, which produced results that confirmed the correct implementation of said methods. Moreover, the tests were conducted on PWR assemblies which are known to work extraordinarily well with the diffusion equation. As such, we cannot boast that the transport SPH produces better results than the diffusion SPH and has the merit to be used at every occasion. The SPH method, which traditionally relied on a fixed-point, Picard, iteration scheme was also solved using a PJFNK method, greatly diminishing the calculation time while producing better converged results. However, the PJFNK SPH method relies on having an initial guess within the radius of convergence of the Newton method to reach convergence. When this is not the case, we have devised a combination of the SPH iteration with the SPH PJFNK to use "Free SPH Iterations" to improve the initial solution which should allow convergence. Because of this, we strongly recommend the PJFNK SPH method over the traditional iterative scheme.

To test the capability of this new SPH procedure, a simplified PWR core was modeled including 15 fuel assemblies, water reflectors and vacuum boundary conditions. The SPH method is known to not reach convergence in these types of problem, but the SPH procedure we implemented rapidly converged for the the SPH iterative scheme and PJFNK method. This may be explained by the fact that the SPH iteration scheme relies on the PJFNK method to solve the linear equations at each iteration. Moreover, the PJFNK SPH method converged much more quickly, proving the versatility of this method. A study was also conducted using a simplified model of INL's TREAT reactor, which contains very large graphite reflector regions, vacuum boundary conditions and a very important control rod effect. The PJFNK SPH procedure with free iterations converged the problem and produced RMS errors well within 1%. This problem demonstrated the strength of the SPH PJFNK method by having such important reflector regions while also producing very high fidelity results when it comes to reaction rates and power distributions.

5.2 New Uses of the SPH Procedure

The SPH method was previously known to have issues when it comes to reflector regions and void boundary conditions. Using the PJFNK SPH method, these problems have been treated with very good results. This novel method of solving the SPH equations will allow full reactors to be accurately homogenized to produce results that are more consistent with reality since this new method is much faster and reliable than the SPH iterative process. The SPH correction was also applied to the neutron transport equation and tested with P_N and S_N. The results indicate that the SPH method also works for transport schemes, which opens the possibilities of using this type of correction in codes which primarely use the discrete ordinates method or for problems in which the diffusion approximation no longer holds.

5.3 Future Research Avenues

The SPH correction of the neutron transport equation has been shown to work for more complex problems in this thesis. However, the method was tested on PWR assemblies, which are modeled extremely well through diffusion. As such, we were not able to demonstrate the full power of the SPH corrected transport equations. An interesting research avenue would be to use the SPH corrected transport equations on problems in which the diffusion approximation does not hold and where high order S_N or P_N are needed, such as fast breeder reactor (FBR) lattices.

The PJFNK SPH method has already been shown to be very robust and to be able to correct big problems with large reflector regions and vacuum boundary conditions. However, these results were obtained through simplified models of actual reactors. As such, the application of SPH on a full core seems to be the next step in the advancement of the SPH method. However, a use for this needs to be found since the full reference values are needed. We believe that producing high fidelity results from SPH correction can be of great uses when we consider multi-physics applications, such as heat exchange or fuel performance, or in the use of time-dependent reactor analysis. For example, a full reference calculation may be obtained for the beginning of a transient simulation which is then SPH corrected to be used in a deterministic time-dependent solver. This can be very useful since Monte Carlo codes are still very slow at performing time-dependent nuclear physics simulations when compared to deterministic codes.

REFERENCES

Alain Hébert, *Applied Reactor Physics*, 2nd ed. Montréal, Canada: Presses Internationales Polytechnique, 2016.

——, "Développement de la méthode SPH : Homogénéisation de cellules dans un réseau non uniforme et calcul des paramètres de réflecteur," Ph.D. dissertation, CEA-N-2209, Sep. 1981.

S. Balay, S. Abhyankar, M. F. Adams, J. Brown, P. Brune, K. Buschelman, L. Dalcin, V. Eijkhout, W. D. Gropp, D. Kaushik, M. G. Knepley, L. C. McInnes, K. Rupp, B. F. Smith, S. Zampini, and H. Zhang, "PETSc Web page," http://www.mcs.anl.gov/petsc, 2015. [Online]. Available: http://www.mcs.anl.gov/petsc

Y. Berman, "An improved homogenization technique for pin-by-pin diffusion calculations," *Annals of Nuclear Energy*, vol. 53, no. 53, pp. 238 – 243, 2013.

R. A. Berry, J. W. Peterson *et al.*, "RELAP-7 theory manual," Idaho National Laboratory, Tech. Rep., 2014.

R. Chambon and A. Hébert, "A new open-source pin power reconstruction capability in DRAGON5 and DONJON5 neutronic codes," *Nuclear Engineering and Design*, vol. 289, no. 289, pp. 208 – 217, 2015.

G. Chiba, M. Tsuji, K. Sugiyama, and T. Narabayashi, "A note on application of superhomogénéisation factors to integro-differential neutron transport equations," *Journal of Nuclear Science and Technology*, vol. 49, no. 2, pp. 272–280, 2012.

M. Fliscounakis, E. Girardi, and T. Courau, "A generalized pin-power reconstruction method for arbitrary heterogeneous geometries," in *International Conference on Mathematics and Computational Methods Applied (MC 2011)*. Rio de Janeiro, RJ, Brazil: American Nuclear Society, May 2011.

T. Fujita, T. Endo, and A. Yamamoto, "Application of correction technique using leakage index combined with SPH or discontinuity factors for energy collapsing on pin-by-pin BWR core analysis," *Journal of Nuclear Science and Technology*, vol. 52, no. 3, pp. 355–370, 2015.

D. Gaston, C. Newman, G. Hansen, and D. Lebrun-Grandié, "MOOSE: A parallel computational framework for coupled systems of nonlinear equations," *Nuclear Engineering and Design*, vol. 239, no. 10, pp. 1768 – 1778, 2009.

D. Gaston *et al.*, "Continuous integration for concurrent computational framework and application development," *Journal of Open Research Software*, vol. 2, no. 1, p. e10, 2014.

F. Gleicher, J. Ortensi *et al.*, "The coupling of the neutron transport application RATTLESNAKE to the fuels perfomance application BISON," in *International Conference on Reactor Physics (PHYSOR 2014)*, Kyoto, Japan, 2014.

U. Grundmann and S. Mittag, "Super-homogenisation factors in pinwise calculations by the reactor dynamics code dyn3d," *Annals of Nuclear Energy*, vol. 38, no. 10, pp. 2111 – 2119, 2011.

P. Guerin, T. Courau, D. Couyras, and E. Girardi, "Equivalence et correction de transport dans COCAGNE," EDF - RD, Tech. Rep., 2011.

A. Hébert, "A reformulation of the transport-transport SPH equivalence technique," no. 7. 7ICMSNSE, 2015.

A. Hébert, "A consistent technique for the pin-by-pin homogenization of a pressurized water reactor assembly," *Nuclear Science and Engineering*, vol. 113, no. 3, pp. 227–238, March 1993.

A. Hébert and P. Benoist, "A consistent technique for the global homogenization of a pressurized water reactor assembly," *Nuclear Science and Engineering*, vol. 109, no. 4, pp. 360–372, December 1991.

A. Hébert and G. Mathonnière, "Development of a third-generation superhomogeneisation method for the homogenization of a pressurized water reactor assembly," *Nuclear Science and Engineering*, vol. 115, no. 2, pp. 129–141, October 1993.

N. Horelik, B. Herman, B. Forget, and K. Smith, "Benchmark for evaluation and validation of reactor simulations (BEAVRS)," Sun Valley, Idaho, 2013.

IAEA, "Evaluation of high temperature gas cooled reactor performance: Benchmark analysis related to initial testing of the HTTR and HTR-10," International Atomic Energy Agency, Tech. Rep., 2003.

A. Kavenoky, "The SPH homogenization method," Lugano, November 1978, TECDOC.

D. Knoll and D. Keyes, "Jacobian-free Newton–Krylov methods: a survey of approaches and applications," *Journal of Computational Physics*, vol. 193, no. 2, pp. 357 – 397, 2004.

J. Leppänen, "Serpent– a continuous-energy Monte Carlo reactor physics burnup calculation code." VTT Technical Research Centre of Finland, Tech. Rep., 2015.

M. Li, K. Wang, and D. Yao, "The super equivalence method in Monte Carlo based homogenization," no. 22, Proceedings of the 2014 22nd International Conference on Nuclear Engineering. ICONE22, July 2014.

J. Ma, G. Wang, S. Yuan, H. Huang, and D. Qian, "An improved assembly homogenization approach for plate-type research reactor," *Annals of Nuclear Energy*, vol. 85, pp. 1003 – 1013, 2015.

G. Marleau, A. Hébert, and R. Roy, "A USER GUIDE for DRAGON version5. Report IGE-355," École Polytechnique de Montréal, Tech. Rep., 2014.

E. Nikitin, E. Fridman, and K. Mikityuk, "On the use of the SPH method in nodal diffusion analyses of SFR cores," *Annals of Nuclear Energy*, vol. 85, pp. 544 – 551, 2015.

J. Ortensi *et al.*, "Preparation of a neutron transport data set for simulations of the transient test reactor facility," in *PHYSOR-2016, ANS Topical Meeting on Reactor Physics*, Sun Valley, Idaho, USA, 2016.

A. Pautz, "Improved strategies for fuel assemly, pin cell and reflector cross section generation using the discrete ordinates code DORT," in *PHYSOR-2006, ANS Topical Meeting on Reactor Physics*, Vancouver, BC, Canada, September 2006.

J. Ragusa, R. Sanchez, and S. Santandrea, "Application of duality principles to reflector homogenization," *Nuclear Science and Engineering*, vol. 157, no. 2, pp. 299–315, 2007.

J. Rhodes, K. Smith, and D. Lee, "CASMO-5 development and applications," in *PHYSOR-2006, ANS Topical Meeting on Reactor Physics*, Vancouver, BC, Canada, 2006.

R. Sanchez, "Assembly homogenization techniques for core calculations," *Progress in Nuclear Energy*, vol. 51, no. 1, pp. 14 – 31, 2009.

K. Smith, "Assembly homogenization techniques for light water reactor analysis," *Progress in Nuclear Energy*, vol. 17, no. 3, pp. 303 – 335, 1986.

Y. Wang, "Nonlinear diffusion acceleration for the multigroup transport equation discretized with S_N and continuous FEM with RATTLESNAKE," in *Proceedings to the International Conference on Mathematics, Computational Methods & Reactor Physics (M&C 2013)*, Sun Valley, Idaho, USA, 2013.

R. Williamson *et al.*, "Multidimensional multi-physics simulations of nuclear fuel behaviour," *Journal of Nuclear Materials*, vol. 423, pp. 149 – 163, 2012.

A. Yamamoto, Y. Kitamura, and Y. Yamane, "Cell homogenization methods for pin-by-pin core calculations tested in slab geometry," *Annals of Nuclear Energy*, vol. 31, no. 8, pp. 825 – 847, 2004.

A. Yamamoto, M. Tatsumi, Y. Kitamura, and Y. Yamane, "Improvement of the SPH method for pin-by-pin core calculations," *Journal of Nuclear Science and Technology*, vol. 41, no. 12, pp. 1155–1165, 2004.

APPENDIX A THE EVEN AND ODD NEUTRON TRANSPORT EQUATIONS

The multi-group steady-state neutron transport equation is written as:

$$\vec{\Omega}\cdot\vec{\nabla}\Psi_g(\vec{x},\vec{\Omega})+\Sigma_g^t(\vec{x})\Psi_g(\vec{x},\vec{\Omega})= \sum_{g'}^{G}\int_{4\pi}d\Omega'\Sigma_s^{g\leftarrow g'}(\vec{x},\vec{\Omega}'\cdot\vec{\Omega})\Psi_{g'}(\vec{x},\vec{\Omega}')+\frac{\chi_g}{k_{eff}}\sum_{g'}^{G}\int_{4\pi}d\Omega'\nu\Sigma_{f_{g'}}(\vec{x})\Psi_{g'}(\vec{x},\vec{\Omega}') \quad \text{(A.1)}$$

Equation A.1 can also be written with negative parity by setting $\Omega\rightarrow-\Omega$:

$$-\vec{\Omega}\cdot\vec{\nabla}\Psi_g(\vec{x},-\vec{\Omega})+\Sigma_g^t(\vec{x})\Psi_g(\vec{x},-\vec{\Omega})= \sum_{g'}^{G}\int_{4\pi}d\Omega'\Sigma_s^{g\leftarrow g'}(\vec{x},\vec{\Omega}'\cdot-\vec{\Omega})\Psi_{g'}(\vec{x},\vec{\Omega}')+\frac{\chi_g}{k_{eff}}\sum_{g'}^{G}\int_{4\pi}d\Omega'\nu\Sigma_{f_{g'}}(\vec{x})\Psi_{g'}(\vec{x},\vec{\Omega}') \quad \text{(A.2)}$$

Both previous equations are added together and divided by 2 to obtain:

$$\begin{aligned}&\vec{\Omega}\cdot\vec{\nabla}\frac{\left(\Psi_g(\vec{x},\vec{\Omega})-\Psi_g(\vec{x},-\vec{\Omega})\right)}{2}+\Sigma_g^t(\vec{x})\frac{\left(\Psi_g(\vec{x},\vec{\Omega})+\Psi_g(\vec{x},-\vec{\Omega})\right)}{2}= \\ &\sum_{g'}^{G}\int_{4\pi}d\Omega'\frac{\left(\Sigma_s^{g\leftarrow g'}(\vec{x},\vec{\Omega}'\cdot\vec{\Omega})+\Sigma_s^{g\leftarrow g'}(\vec{x},\vec{\Omega}'\cdot-\vec{\Omega})\right)}{2}\Psi_{g'}(\vec{x},\vec{\Omega}') \\ &+\frac{\chi_g}{k_{eff}}\sum_{g'}^{G}\int_{4\pi}d\Omega'\nu\Sigma_{f_{g'}}(\vec{x})\Psi_{g'}(\vec{x},\vec{\Omega}')\end{aligned} \quad \text{(A.3)}$$

Equation A.2 is substracted from A.1 and divided by 2 to obtain:

$$\begin{aligned}&\vec{\Omega}\cdot\vec{\nabla}\frac{\left(\Psi_g(\vec{x},\vec{\Omega})+\Psi_g(\vec{x},-\vec{\Omega})\right)}{2}+\Sigma_g^t(\vec{x})\frac{\left(\Psi_g(\vec{x},\vec{\Omega})-\Psi_g(\vec{x},-\vec{\Omega})\right)}{2}= \\ &\sum_{g'}^{G}\int_{4\pi}d\Omega'\frac{\left(\Sigma_s^{g\leftarrow g'}(\vec{x},\vec{\Omega}'\cdot\vec{\Omega})-\Sigma_s^{g\leftarrow g'}(\vec{x},\vec{\Omega}'\cdot-\vec{\Omega})\right)}{2}\Psi_{g'}(\vec{x},\vec{\Omega}')\end{aligned} \quad \text{(A.4)}$$

where the even and odd fluxes are defined as:

$$\Psi_g^{even}(\vec{x},\vec{\Omega}) = \frac{\Big(\Psi_g(\vec{x},\vec{\Omega}) + \Psi_g(\vec{x},-\vec{\Omega})\Big)}{2} \tag{A.5}$$

$$\Psi_g^{odd}(\vec{x},\vec{\Omega}) = \frac{\Big(\Psi_g(\vec{x},\vec{\Omega}) - \Psi_g(\vec{x},-\vec{\Omega})\Big)}{2} \tag{A.6}$$

and the even and odd scattering cross sections:

$$\Sigma_s^{g\leftarrow g'}(\vec{x},\vec{\Omega}'\cdot\vec{\Omega})^{even} = \frac{\Big(\Sigma_s^{g\leftarrow g'}(\vec{x},\vec{\Omega}'\cdot\vec{\Omega}) + \Sigma_s^{g\leftarrow g'}(\vec{x},\vec{\Omega}'\cdot-\vec{\Omega})\Big)}{2} \tag{A.7}$$

$$\Sigma_s^{g\leftarrow g'}(\vec{x},\vec{\Omega}'\cdot\vec{\Omega})^{odd} = \frac{\Big(\Sigma_s^{g\leftarrow g'}(\vec{x},\vec{\Omega}'\cdot\vec{\Omega}) - \Sigma_s^{g\leftarrow g'}(\vec{x},\vec{\Omega}'\cdot-\vec{\Omega})\Big)}{2} \tag{A.8}$$

to finally obtain the even and odd parity neutron transport equations:

$$\begin{aligned} even\ parity\ :\ & \vec{\Omega}\cdot\vec{\nabla}\Psi_g^{odd}(\vec{x},\vec{\Omega}) + \Sigma_g^t(\vec{x})\Psi_g^{even}(\vec{x},\vec{\Omega}) = \\ & \sum_{g'}^{G}\int_{4\pi} d\Omega' \Sigma_s^{g\leftarrow g'}(\vec{x},\vec{\Omega}'\cdot\vec{\Omega})^{even}\Psi_{g'}(\vec{x},\vec{\Omega}') \\ & + \frac{\chi_g}{k_{eff}}\sum_{g'}^{G}\int_{4\pi} d\Omega' \nu\Sigma_{f_{g'}}(\vec{x})\Psi_{g'}(\vec{x},\vec{\Omega}') \end{aligned} \tag{A.9}$$

$$\begin{aligned} odd\ parity\ :\ & \vec{\Omega}\cdot\vec{\nabla}\Psi_g^{even}(\vec{x},\vec{\Omega}) + \Sigma_g^t(\vec{x})\Psi_g^{odd}(\vec{x},\vec{\Omega}) = \\ & \sum_{g'}^{G}\int_{4\pi} d\Omega' \Sigma_s^{g\leftarrow g'}(\vec{x},\vec{\Omega}'\cdot\vec{\Omega})^{odd}\Psi_{g'}(\vec{x},\vec{\Omega}') \end{aligned} \tag{A.10}$$

The integral over the angles can be expanded into a summation of spherical harmonics, the P_N method:

$$\int_{4\pi} d\Omega' \Sigma_x^g(\vec{x},\vec{\Omega}',\vec{\Omega})\Psi_g(\vec{x},\vec{\Omega}') = \sum_{\ell=0}^{\infty}\frac{2\ell+1}{4\pi}\sum_{n=-\ell}^{\ell}\Sigma_{x,\ell}^g(\vec{x})\phi_{g,\ell,n}(\vec{x})Y_{\ell,n}(\vec{\Omega}) \tag{A.11}$$

In this thesis, we use the indexes ℓ and n for the spherical harmonics instead of ℓ and m as

we use the index m as an indicator of a homogenized region. This sum notation is then used to get rid of the integrals:

$$\begin{aligned} \textit{even parity} \ : \ & \vec{\Omega}\cdot\vec{\nabla}\Psi_g^{odd}(\vec{x},\vec{\Omega}) + \Sigma_g^t(\vec{x})\Psi_g^{even}(\vec{x},\vec{\Omega}) = \\ & \sum_{g'}^{G}\sum_{\ell}^{\infty}\sum_{even}\frac{2\ell+1}{4\pi}\sum_{n=-\ell}^{\ell}\Sigma_{s,\ell}^{g\leftarrow g'}(\vec{x})\phi_{g',\ell,n}(\vec{x})Y_{\ell,n}(\vec{\Omega}) \\ & + \frac{\chi_g}{k_{eff}}\sum_{g'}^{G}\sum_{\ell}^{\infty}\sum_{even}\frac{2\ell+1}{4\pi}\sum_{n=-\ell}^{\ell}\nu\Sigma_{f,\ell_{g'}}(\vec{x})\phi_{g',\ell,n}(\vec{x})Y_{\ell,n}(\vec{\Omega}) \end{aligned} \tag{A.12}$$

$$\begin{aligned} \textit{odd parity} \ : \ & \vec{\Omega}\cdot\vec{\nabla}\Psi_g^{even}(\vec{x},\vec{\Omega}) + \Sigma_g^t(\vec{x})\Psi_g^{odd}(\vec{x},\vec{\Omega}) = \\ & \sum_{g'}^{G}\sum_{\ell}^{\infty}\sum_{odd}\frac{2\ell+1}{4\pi}\sum_{n=-\ell}^{\ell}\Sigma_{s,\ell}^{g\leftarrow g'}(\vec{x})\phi_{g',\ell,n}(\vec{x})Y_{\ell,n}(\vec{\Omega}) \end{aligned} \tag{A.13}$$

where the classic definition of the real spherical harmonics is adopted:

$$Y_{0,0} = 1. \tag{A.14}$$

Since fission is isotropic, only the zeroth order term contributes to the sum. ϕ_g is used as shorthand notation for $\phi_{g,0,0}$. The even and odd parity neutron transport equations are finally obtained:

$$\begin{aligned} \textit{even parity} \ : \ & \vec{\Omega}\cdot\vec{\nabla}\Psi_g^{odd}(\vec{x},\vec{\Omega}) + \Sigma_g^t(\vec{x})\Psi_g^{even}(\vec{x},\vec{\Omega}) = \\ & \sum_{g'}^{G}\sum_{\ell}^{\infty}\sum_{even}\frac{2\ell+1}{4\pi}\sum_{n=-\ell}^{\ell}\Sigma_{s,\ell}^{g\leftarrow g'}(\vec{x})\phi_{g',\ell,n}(\vec{x})Y_{\ell,n}(\vec{\Omega}) \\ & + \frac{\chi_g}{4\pi}\frac{1}{k_{eff}}\sum_{g'}^{G}\nu\Sigma_{f_{g'}}(\vec{x})\phi_{g'}(\vec{x}) \end{aligned} \tag{A.15}$$

$$\begin{aligned} \textit{odd parity} \ : \ & \vec{\Omega}\cdot\vec{\nabla}\Psi_g^{even}(\vec{x},\vec{\Omega}) + \Sigma_g^t(\vec{x})\Psi_g^{odd}(\vec{x},\vec{\Omega}) = \\ & \sum_{g'}^{G}\sum_{\ell}^{\infty}\sum_{odd}\frac{2\ell+1}{4\pi}\sum_{n=-\ell}^{\ell}\Sigma_{s,\ell}^{g\leftarrow g'}(\vec{x})\phi_{g',\ell,n}(\vec{x})Y_{\ell,n}(\vec{\Omega}) \end{aligned} \tag{A.16}$$